Budapest University of Technology and Economics
Faculty of Mechanical Engineering

Department of Fluid Mechanics

Investigation of vortex-induced vibrations using OpenFOAM

BACHELOR'S THESIS

Author:
Yifan Luo

Supervisor:
Dr. Josh Davidson
Research Fellow

Budapest, 2021

Declarations

Declaration of acceptance

This thesis fulfills all formal and content requirements prescribed by the Faculty of Mechanical Engineering of Budapest University of Technology and Economics, as well as it fully complies all tasks specified in the transcript. I consider this thesis as it is suitable for submission for public review and for public presentation.

Done at Budapest, 13.12.2019

Dr. Josh Davidson

Declaration of independent work

I, Yifan Luo, the undersigned, hereby declare that the present thesis work has been prepared by myself without any unauthorized help or assistance such that only the specified sources (references, tools, etc.) were used. All parts taken from other sources word by word or after rephrasing but with identical meaning were unambiguously identified with explicit reference to the sources utilized.

Done at Budapest, 13.12.2019

Yifan Luo

Acknowledgements

First and foremost, I would like to thank God, the almighty, my father in heaven, for all the blessings, for always being there, walking along side me throughout all my deepest valley. May all the glory be to God.

I would also like to thank my supervisor, Dr. Josh Davidson, for his professionalism, patience, and all the supports he have provided during the research. I had limited knowledge with the particular tools to be used to complete this research, along with how a proper thesis should look like in the very beginning. But with the help from my supervisor those have not been any problem anymore. It is not only for the sake of the thesis that I thank Dr. Josh Davidson for, but also the knowledge that have been brought to me and became my own. It has been a privilege to work with him.

I would like to express my gratitude and thanks to my family. Without their support, there is no way I could manage to get this far. Even that we have been apart because of my study aboard for almost six years now, it is the never changing love, support, and trust that have always been taking care of me.

I would like to thank Pastor Dan Dunbar and Pastor Graham King for they have brought me out of my struggles, covering me and praying for me.

Last but not least, I would like to give my special thanks to my girlfriend, Weiwei Fan, along side with my friends, Kangjian Huang, Qiaoyi Li, Xiaobao Hui, Zijian Li and Peng Jiang. Friends are important, especially when studying aboard. Therefore, I would like to thank them for their support.

Abstract

Vortex induced vibration (VIV) is one of the most concerning phenomenon when comes to the interaction between fluid and solid. It is especially most practical for those that have a geometrically low aspect ratio, for example skyscrapers and bridges. The study regarding VIV has a history well over fifty years, but even till this day, the behavior of this phenomenon is not yet fully defined. This thesis focus on investigating the behavior of this phenomenon with OpenFOAM with controlled velocity, shape, mass, fluid property, and natural frequency. With the numerical results obtained, frequency ratio, amplitude ratio, settling time, and critical value are investigated with a variable mass.

Keywords: *vortex induced vibration, vortex shedding, OpenFOAM*

Contents

Chapter 1

Introduction

1.1 Basic Principles of VIV

The study of vortex-induced vibration (VIV) can be found useful and practical in many engineering fields. It represents one of the most concerning issues for bluff bodies in air and water. In fluid dynamics, VIV occurs when shedding vortices (produced by any flow passing a body) apply oscillatory force on the body. The shedding vortices generate pulsating pressure on the body that changes periodically in the parallel and perpendicular directions of the flow. Suppose the body is elastically supported, or the material is flexible and allows elastic deformation. In that case, the oscillatory force will trigger periodic vibration of the body, and this vibration will, in turn, change the wake pattern of the vortex. Generally, there are three wake patterns close to the "lock-in" range of VIV: 2 singles, 2 pairs, and pair plus single[1][2]. The VIV phenomenon only happens in a limited range of reduced flow velocity (U^*) and disappears at higher flow velocities. It is also worth noting that once the Reynolds number is high enough, VIV will not only occur in cylinders but also on all bluff bodies with oscillating wakes.

The vortex shedding frequency (f) produced by a stationary body encountering a flow is proportional to the flow velocity (U) and inversely proportional to the characteristic dimension (D) of the body (for instance, diameter of cylinder)[3].

$$f = S\frac{U}{D} \tag{1.1}$$

The Strouhal number (St) is the constant of proportionality. However, as the equations demonstrate, VIV is not a simple linear forced vibration. Since the body is elastically mounted, a "lock-in" participates in the response of frequency changes. This actively demonstrates that the body's vibration is causing f^* to stay around 1, causing the resonance range in respect of flow velocity to extend. The phenomenon of "lock-in" generally means that after the vortex shedding frequency (f) becomes close to the body's natural frequency (f_N), where $f^* = f/f_N \approx 1$. The shedding frequency will remain close to the body's natural frequency as velocity increases in a limited range called the lock-in range. This phenomenon causes the amplitude of the oscillation to be increasing after f first

Mass ratio	m^*	$\frac{m}{\pi\rho D^2 L/4}$
Damping ratio	ζ	$\frac{c}{2\sqrt{k(m+m_A)}}$
Velocity ratio	U^*	$\frac{U}{f_n D}$
Amplitude ratio	Y^*	$\frac{y_0}{D}$
Frequency ratio	f^*	$\frac{f}{f_n}$
Streamwise force coef.	K_X	$\frac{F_X}{\frac{1}{2}\rho U^2 DL}$
Transverse force coef.	K_Y	$\frac{F_y}{\frac{1}{2}\rho U^2 DL}$
Reynolds number	Re	$\frac{\rho U D}{v}$

Table 1.1: Non-dimensional parameters

reaches f_N instead of decreasing as the usual should have been. However, considerably huge multiple times of the natural frequency can be reached for the VIV frequency as recent study has shown.

To begin the study of VIV and in order to understand the fundamental questions relating to this subject, we introduce the generally used equation of motion that express VIV of a cylinder elastically mounted and vibrating in the transverse direction:

$$my'' + cy' + ky = F \tag{1.2}$$

where c is the structural damping, m is the structural mass, k is the spring constant, and F is the fluid force in the transverse direction. A well established numerical solution of the force and the amplitude can be expressed as:

$$F(t) = F_0 sin(\omega t + \phi) \tag{1.3}$$

$$y(t) = y_0 sin(\omega t) \tag{1.4}$$

where ω is $2\pi f$, and f is the body's oscillation frequency. Having these three equation defined, the amplitude and frequency of the oscillation can be derived as follow using non-dimensional parameters[4]:

$$Y^* = \frac{1}{4\pi^3} \frac{K_{Y sin\Phi}}{(m^* + K_A)\sigma} (\frac{U^*}{f^*}) f^* \tag{1.5}$$

$$f^* = \sqrt{\frac{m^* + K_A}{m^* + K_{EA}}} \tag{1.6}$$

where K_A is the potential added mass coefficient (taking the value as 1) and K_{EA} is the actual added mass coefficient that includes the effect due to the force applied from the fluid and can be calculated as (of course, K_{EA} is not a mass since there are apparent force components):

$$K_{EA} = \frac{1}{2\pi^3} \frac{K_{Y cos\Phi}}{Y^*} (\frac{U^*}{f^*}) \tag{1.7}$$

With these equations in mind, studies and modeling had been made. A study of the response for an elastically mounted cylinder was made by Feng[5] and has contributed to the subject. In his research, he found and defined two different branches for the response, which he called the "initial" and "lower" branches (as shown in Figure 1.1). Air was used in the experiment as the fluid, so that it made the mass ratio very big ($m^* \sim 250$). However, more recent studies have been made with lower mass ratios using water as the fluid. One of the comparisons was done with research from Khalak and Williamson[6] between the amplitude in water ($m^* = 2.4$) and the highest amplitude that Feng has plotted in air (Figure 1.1a). This comparison research has a value of $m^*\zeta$, only about 3% of Feng's value, which in result yields a much higher peak amplitude. Several studies by Khalak and Williamson had shown a new category between the initial and lower, a much higher branch called the "upper response branch". Along with the maximum amplitude difference due to the much lower mass ratio, another contrasting result was found with the synchronized frequency during the "lock-in". In the case of a light body in water, the body vibrates at 1.4 times the natural frequency.

1.2 Critical Mass

From the results discussed above, some may easily conclude that as the object's mass decreases, the amplitude of vibration for a given flow velocity will increase. However, this simultaneity rule tends to reach boundlessly vast when the mass is under a unique critical value, other than when the mass reaches zero. The critical point is dependent on the body's shape that's under the phenomenon of VIV. Govardhan and Williamson[8] presented an extensive research for cylinders with low mass damping to determine K_{EA} that is not changing the whole time with the lower category rule and is independent of m^*. They found the most suitable representation of K_{EA} in Equation 1.6, where the research data of their own fits the most (Figure 1.2, which is, $K_{EA} = -0.54 \pm 0.02$.

Therefore, the lower-branch frequency Equation 1.6 can be deduced as following:

$$f^*_{Lower} = \sqrt{\frac{m^* + K_A}{m^* - 0.54}} \tag{1.8}$$

where $K_A = 1$. The expression for f^*_{Lower} in Equation 1.8 is mathematically straightforward that when the critical mass tends to reach 0.54, the frequency ratio of the lower branch becomes infinity. This also gives the simplest way of calculating the maximum frequency in this branch. Therefore Govardhan and Williamson proves that critical mass ratio is definitely real can can be defined as:

$$m^*_{Critical} = 0.54. \tag{1.9}$$

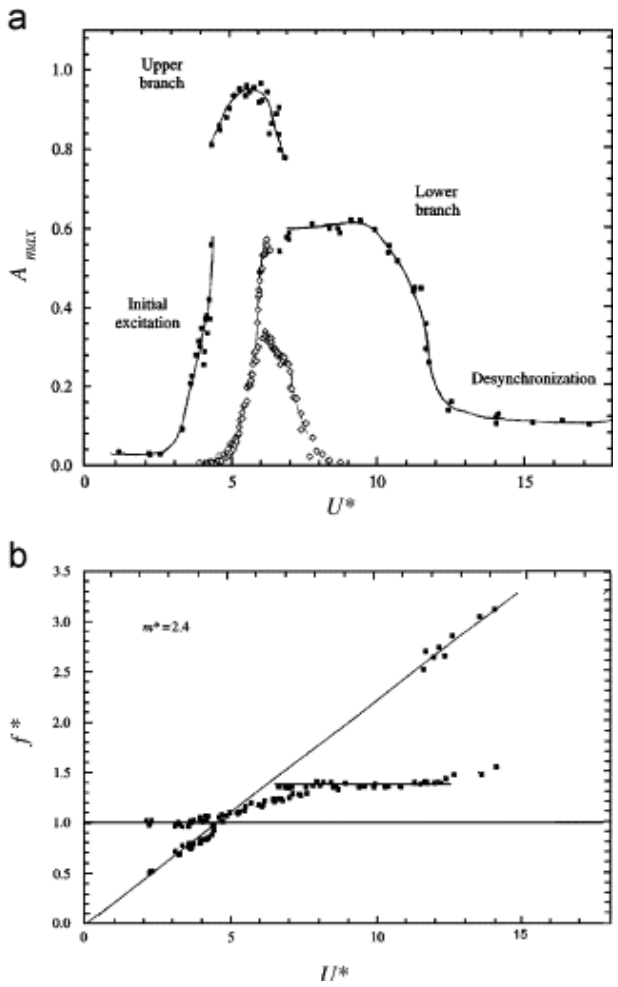

Figure 1.1: In (a), Feng's result of maximum amplitude with high mass ratio is compared with with Khalak and Williamson's result with low mass ratio. In (b), the frequency is not close to the natural frequency as the classic result expected[6][7].

The result is significant, but one thing to notice is that this experiment is carried only under a certain condition. Where the mass damping is low. In fact they have stated that this critical mass only valid when the product of mass and damping is lower than 0.05.

For frequency of the upper category, a study had been done by Govardhan and Williamson[11] following their study of the lower branch. The frequency ratio f^* is shown to increase with the reduced velocity, starting from the reduced velocity of 5 and the frequency ratio of 1 (Figure 1.3a). It should theoretically stop when it reaches the lower branch, but as the experiment has shown, it is not clear if the frequency will jump back to the lower branch. In fact, the ones who actually performed this experiment stated that the upper branch will continue endlessly. The response curve of the measurement done with $m^* = 0.52$ is shown in Figure 1.3. Although the curve is limited by the equipment, it is pretty clear that the amplitude of the vibration tends to stay at a high level even compared to $m^* = 8.63$'s case.

Further studies have been made relating the critical mass of a VIV system. Reducing the mass has a significant effect on how the system will respond. When the mass ratio has been reduced under the discovered critical value, enormous amplitude and intensive

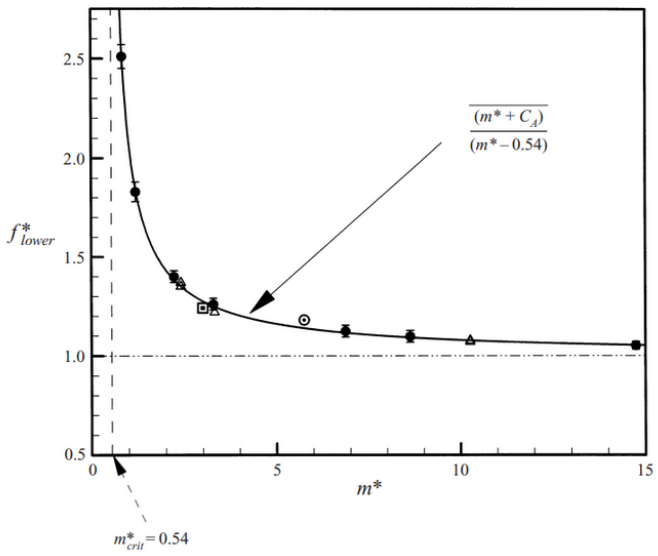

Figure 1.2: The oscillation frequency for lower branch represented by the mass ratio m^*. It is shown that K_{EA} value of 0.54 fits remarkably well. The symbols representing the data are: •, Govardhan and Williamson[8]; △, Khalak and Williamson[4]; ⊡, Hover, et al.[9]; ⊙, Anand and Torum[10].

vibration occur. When the system operates within these circumstances, the phenomenon of VIV may occur at any given velocity, which means that the object will constantly be vibrating (Figure 1.3b).

There follows other similar studies which focus on the critical mass of different shapes under VIV. Govardhan and Williamson[11] wrote about how a critical value should lay on any type of VIV. As Williamson and his colleagues have done more studies throughout the years, critical masses of many other shapes are found[12][13].

Recent studies have found that critical mass varies with the fluid's Reynolds numbers. A low Reynolds number leads to changes of the critical number. First, Morse & Williamson[14] found that the increase of Reynolds number is taking the critical mass also to increase. In their research, it was determined that as the Reynolds number increases from 4,000 to 30,000, the critical mass ratio has constantly been increasing until 0.54, which yields a difference of around 0.18. Although this result has ruled out the previous studies since none of those considered Reynolds number as a factor, Morse and Williamson state that Reynolds number is a dependent factor of the vital property of mass ratio should have been aware of. When the Reynolds number is small, the influence of the viscous force on the flow field is greater than the inertial force. If the Reynolds number is large, the influence of inertial force on the flow field is greater than the viscous force. The change in force significantly affects the behavior of the system. Then, following their study, Navrose and Sanjay Mittal[15] had made a more comprehensive research on this phenomenon and plotted the whole response curve (Figure 1.4). The detailed calculation and experimental process will not be repeated in this article.

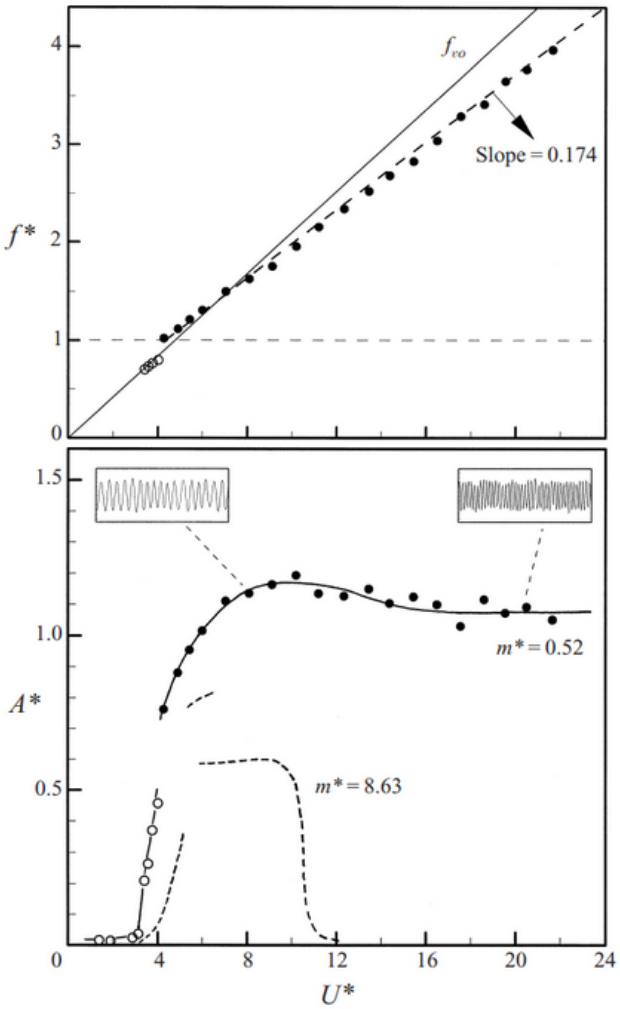

Figure 1.3: In (a), it shows that the frequency ratio has a linear relationship with the velocity ratio. In (b), when m^* is below a critical value, the resonance keeps going until the experiment's equipment's maximum capability[8].

1.3 Response Approximation

Putting aside the critical mass, is there a way to estimate the maximum amplitude of any given body under the phenomenon of VIV? Khalak and Williamson introduced the 'Griffin plot' in their research paper in 1999[4]. Over years of research regarding VIV, the 'Skop-Griffin' parameter was introduced to approximate the maximum amplitude. And it was the most commonly used parameter in many pieces of research. The parameter is essentially closely related to the mass damping ($m^*\zeta$). In fact, it was found proportional to it by Griffin et al.[16]. However, it was still an important question if the parameter could accurately represent the maximum response. Much more research have been done addressing this subject over almost three decades, and no one was able to express the relationship with accuracy. Although people mainly were using a mass and damping related parameter to represent their work, they were not precisely the same. For different shapes of objects, researchers had used several different parameters. Sometimes researchers tend to use a parameter that fits their work the most, even with the same shape. However, all

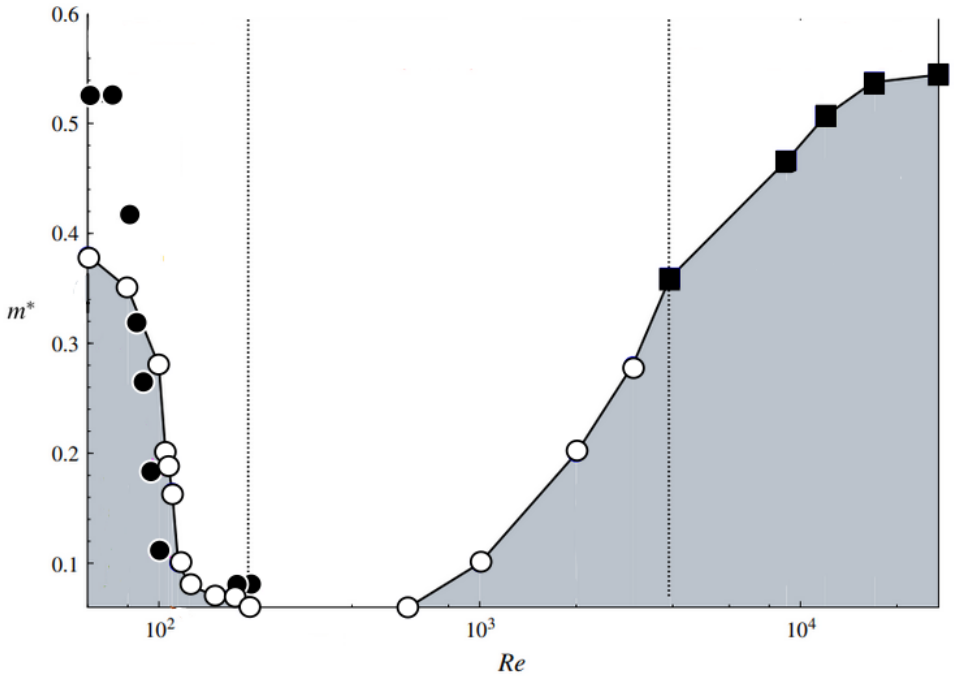

Figure 1.4: Data collected for cylinders by Mittal and Sanjay[15], plotting the critical mass change with Reynolds number. Different notations are from various data sets obtained from previous studies[14]. Under the curve, it shows the area where the phenomenon of VIV occurs boundlessly.

of the parameters were essentially mass damping related. As more and more studies have been done on the maximum amplitude, Skop and Griffin[16] defined a new parameter that combined all of the other research's data. This parameter S_G has been stated to roughly anticipate the response of any VIV system. It is expressed as[17]:

$$S_G = 2\pi^3 S^2(m^*\zeta) \tag{1.10}$$

Griffin et al.[18] first introduced S_G to conduct the extensive compilation of many different studies. Since then, the Griffin plot has been used vastly among research representing the maximum amplitude. Although practical engineers widely use log-log Griffin diagrams[19], it was still not clear with what conditions of flow and frequency it is best suitable, which should have then led to a unique curve between peak amplitude and S_G.

Sarpkaya since then pointed out several times in his researches that the commonly applied parameter S_G's legality[20][21][22][23]. He wrote that even from simple mathematical evaluation from Equation 1.1, the peak amplitude of the system is dependent on both mass and damping separately. Sarpkaya then has also pointed out that the 'Skop-Griffin' parameter is only valid for values under 1. This later was found that it rules most of the plot, as we can see in Figure 1.5.

A study has been done following in 1982, Griffin and his colleague performed a measurement where the 'Skop-Griffin' parameter was under control[31]. Varying the mass ratio from 5 to above 40, they then proved that a lower quality ratio results in the broader synchronization range and expands within a larger normalized speed U^* range.

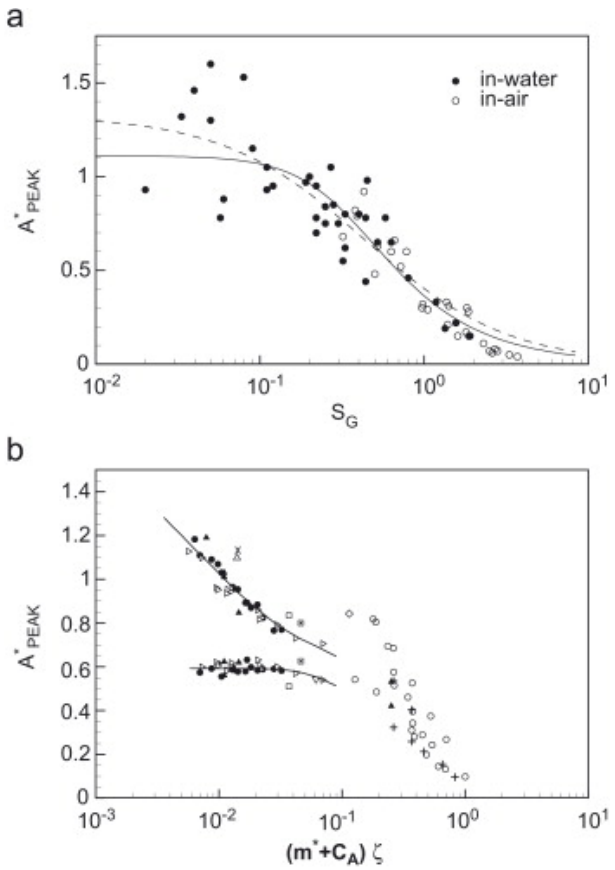

Figure 1.5: Further analysis of the Griffin plot. In (a), the collected data have a quite significant scatter along the fitted line, although it was widely accepted by the researchers at the time. In (b), fitted line is only plotted for a specific geometry and only where the 'Skop-Griffin' parameter is under 1. Although uncertainty is still high, it has improved by quite a lot comparing (a)[4][8][9][19][24][25][12][26][27][28][29][5][30][10].

It also demonstrates that even though $S_G < 1.0$, the parameter and response relationship is not accurate enough, which violates the above-mentioned law stated by Sarpkaya.

For numerous experiments collated by Skop and Balasubramanian[32], Williamson and Govardhan[7] plotted an extension of the Griffin graph. However, instead of the traditional log-log, they adopted a transverse axis (as illustrated in Figure 1.5a). The typical logarithmic relation obscures the dispersion, which is otherwise visible. It appears absurd to combine the data of so many separate VIV systems in this decentralized setting (free cylinder, cantilever, pivot cylinder, and et cetera). As a result, only the data relating to the elastically attached cylinder are shown in Figure 1.5b. Following Khalak and Williamson[4], the Griffin graph has two separate curves that indicate the peak amplitudes of the upper and lower branches, respectively.

Peak-response data was assembled from a variety of different experimental setups, resulting in large uncertainty. The reason of such uncertainty is mostly due to the control method of prior research. However, Govardhan & Williamson[33] used an external active damper to solve this problem. One of the main findings in the study is that when considering Reynolds number (Re) in the relationship between amplitude and the S_G parameter, the data collapse very well. From the study of Govardhan & Williamson, with controlled

damping, They have concluded a equation to predict the amplitude ratio of any given system within a practical range of Reynolds number as:

$$Y^* = (1 - 1.12((m^* + K_A)\zeta) + 0.30((m^* + K_A)\zeta)^2)log(0.41Re^{0.36}) \tag{1.11}$$

Govardhan and Williamson[7] drew a comprehensive graph of amplitude data (Y^*) and mass damping (ζ) measured over the last 30 years, which reveals a considerable dispersion. Because there is no way to differentiate the Re number between each measurement, it's not surprising that it's tough for investigators to verify the data's unique functional connection. (In reality, given this wide range of results, the data cannot support conclusions on whether the combined mass damping parameter is valid or invalid in any way.) However, if the data is now redrawn using "Modified amplitude" $Y^*_M = Y^*/f(Re)$, all preceding data is elegantly folded onto a curve $g(\alpha)$, as shown in Figure 1.6:

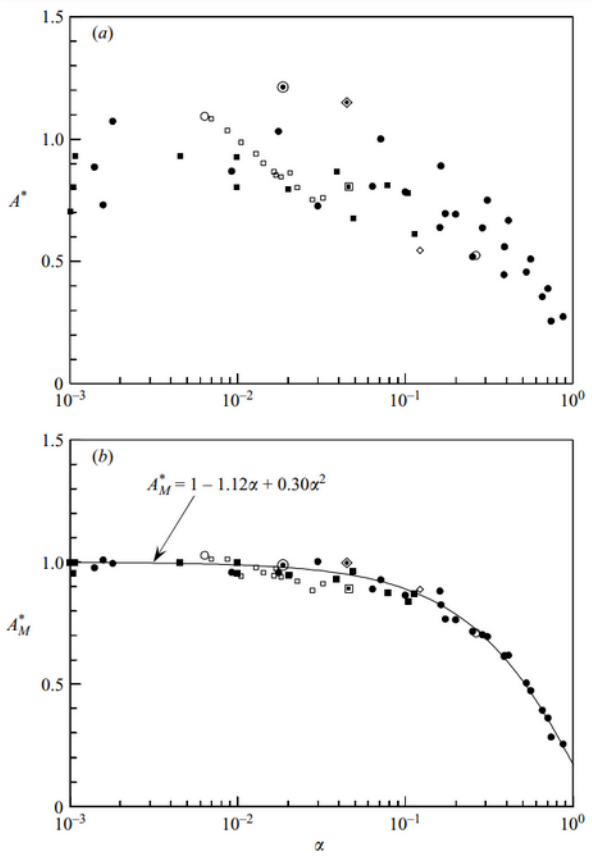

Figure 1.6: With the newly defined relationship including Re, the data produced by all the previous studies collapse elegantly to the fitted line Govardhan and Williamson proposed in 2006[33]. On the top figure, the data plotted with the original Griffin plot. On the bottom figure, the amplitude plotted with respect to the new relationship (Equation 1.11).

1.4 Other Research Results

Although many of the fundamental and basic results about VIV have been discussed, there are undoubtedly much more to discover regarding VIV. Researchers have also been work-

ing on a variety of topics considering the broad applicants of this phenomenon, including forced cylinder vibration, laminar VIV, and XY motion of the bodies. The XY motion here represent flow direction X and transverse Y directions. They will only be mentioned briefly because they are either a more complex problem or are still in development.

In the case of cylinder forced vibration, one way to predict VIV is to create an experimental force database by testing cylinders in free flow that experience forced or controlled sinusoidal vibration. Free vibration testing was compared to prediction using controlled vibration data and hypothetical equations of motion. Hover et al.[34][9] used an ingenious and versatile experiment, a novel force-feedback virtual cable tester (VCTA), in collaboration with Michael Triantafyllou's research team at the Massachusetts Institute of Technology, to produce numerous results. One of the many intriguing findings of this novel device is that, with the exception of the region of maximum amplitude, the impact from both the top and bottom of the object is usually more significant than in the middle. When it comes to predicting VIV, correlation is crucial. Multi-mode motion, traveling waves, and structural non-linearity are all visualized using the general force-feedback system. On the other hand, despite the fact that much work has been done to control vibration, whether control simulations can accurately represent VIV remains an open question.

As far as we know, just one free vibration experiment in the range of laminar vortex shedding was undertaken, which was detailed in Anagnostopoulos & Bearman[35] with a $Re = 90 \sim 150$ range. At $Re = 100 \sim 200$, the response amplitude map also matches the findings of a large number of two-dimensional numerical simulations. It can be inferred that, even in the simulated situation when the damping may be set to zero, there is an evident correlation between the lack of free vibration Y^* and the wake pattern changing to one another when response Y^* surpasses a certain value.

On the other hand, Sarpkaya found that an XY-moving object does not create an unexpected change in the predicted maximum resonance amplitude when compared to a Y-moving object in his research[23]. Later, Jeon & Gharib[36] discovered that even modest quantities of stream-wise motion can prevent the 2P model of vortex generation from forming. Indicating that the amplitudes and phases chosen have an impact on the findings reached. In most situations, cylindrical constructions in the flow direction (X) and transverse (Y) directions have the same mass ratio and natural frequency. The findings reveal that the widespread concept of VIV for only transverse direction body motions has remained tightly linked to the circumstance of two degrees of freedom during the last 35 years. The fluid-structure interaction changes substantially when the mass ratio falls below $m^* = 6$. A "super-upper branch," as described by Jarvis & Williamson[24][12][25], is a new response branch with considerable stream-wise movement. Three large-diameter peak-peak ($Y^*1.5$) amplitudes result from this branch. Following Williamson & Roshko[1], this reaction correlates to a novel periodic vortex wake pattern that includes a triple vortex created in each half-cycle, which is referred to as the "2T" model.

Chapter 2

Methodology

2.1 OpenFOAM

Vortex induced vibration (VIV) is essentially a fluid dynamic problem. Therefore it can be simulated and solved using computational fluid dynamics (CFD). CFD uses numerical methods to solve the control equations of fluid mechanics in the computer to predict the flow of the flow field[37]. At present, there are many kinds of commercial CFD software coming out, such as FLUENT, CFD-ACE+ (CFDRC), Phoenics, CFX, Star-cd, and others. The essential consideration of CFD is to process the continuous fluid in a discrete manner on the computer. One method is to discretize the spatial region into small cells to form a three-dimensional grid or grid point and then apply a suitable algorithm to solve the equation of motion. This process is usually called meshing. Under the consideration of maximum modifiable variances of the simulation, OpenFOAM has become one of the best software capable of this task.

OpenFOAM is an open-source field operation software based on the finite volume method. Its full name is Open Field Operation and Manipulation, and its predecessor is FOAM. The initial class comes from the doctoral dissertation of Charlie Hill (1993), the numerical work comes from Henry Weller (1996) and Hrvoje (1998), and the core of OpenFOAM is a series of high-efficiency C++ module data packages. Based on such data packages, various effective solvers, pre-processing tools (such as meshing, boundary setting, et cetera), and library files (for various models) can be built to simulate specific physical problems and perform pre and post-data processing. At this stage, the platform is mainly used in fluid mechanics or dynamics but has gradually been applied in solid mechanics, including fluid-solid coupling, contact elastoplasticity, nonlinear structural analysis. Throughout years of development under open-source, there are now a considerable amount of solvers, processing tools, and any functionalities available that create a vast amount of freedom setting up the desired solution of any CFD problems[38].

This research aims to recreate the phenomenon of VIV with a cylinder in OpenFOAM under a higher mass damping ($m^*\zeta$) condition and investigate the result's motion behavior. To recreate VIV, it is first necessary to first understand that the vibration is

essentially caused by vortex shedding, and vortex shedding does not occur at any flow speed versus the geometry. Therefore, a stationary case of fluid passing by a cylinder that generates steady vortex shedding is essential for this research.

2.1.1 PimpleFoam

In order to create a simulation case in OpenFOAM, a solver need to be chosen according to case setup and the desired result. The first and most crucial assumption in this research is that the fluid passing by the geometry is incompressible. Also, the solver has to be capable of dealing with turbulence. Therefore, the pimpleFoam solver is chosen under the incompressible fluid solvers category. PimpleFoam is a large-time-step incompressible flow transient solver based on the PIMPLE algorithm, which is a merged algorithm of PISO (Pressure Implicit with Splitting of Operators) and SIMPLE (Semi-Implicit Method for Pressure Linked Equations). Where simpleFoam is a compressible fluid solver with turbulent flow, while pisoFoam is a transient solver for incompressible flow. Essentially, the pimple algorithm is a semi-implicit method for solving pressure and velocity couples[39].

A few solver conditions need to be selected, such as the turbulence model and the controlling of the simulation. There are two commonly used turbulent modeling, RAS and LES. RAS is a very mature model after development in years. But RAS cannot capture the small vortex structure in turbulence after averaging the speed. Unlike RAS, LES examines big vortices while simulating minor vortices at the same time. Large vortices are thought to be directly impacted by boundary conditions, hence LES investigates them; however, tiny vortices are isotropic, so they behave similarly and may be modeled. In this research, the turbulence modeling is set to Large Eddy Simulation (LES). Smagorinsky first proposed LES in 1963, and this method is first used by Dcardorff in a straight calculation field as a numerical simulation. LES separates big vortices and small vortices, then simulates the big one as the model determines the small one. The reason of LES being practical is that there exist inertial sub-scale vortices at a high Reynolds number. The sub-scale vortices can transfer energy in between vortices with energy to those which consume it. However, these vortices themselves do not contain or consume energy in theory. Furthermore, it is suitable for 3D and transient cases. The control of the simulation mainly contains the simulation length, the time interval between each calculation, and the postprocessing methods[40][41].

After the solver has been appropriately set up, the geometry can be easily built. The basic geometry is shown in Figure 2.1. The simulation field is a cuboid with a width of 0.6 m and a length of 0.8 m with a thickness of 0.02 m. In the middle, there is a cylinder with a diameter of 0.04 m. Although the case is set up to be a 3D model, it is basically still a 2D simulation for the reason of mesh distribution that will be mentioned below. The boundary conditions at the layers are set to those which would not disturb the behavior of the fluid and therefore cause any unwanted turbulence. It is important to set only the cylinder boundary to be variable with velocity because this is where the most crucial and

the main focus of this research.

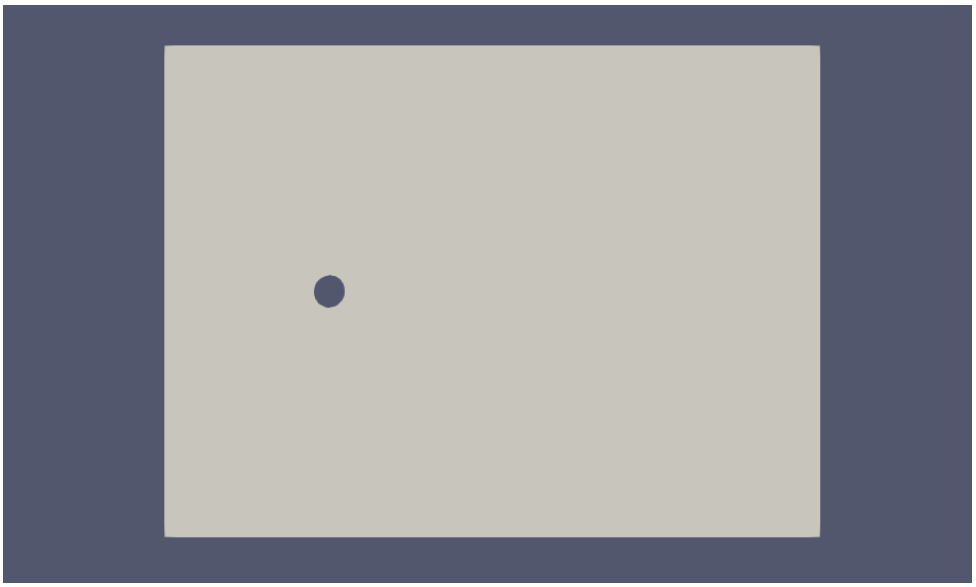

Figure 2.1: The basic geometry of the simulation setup, the inlet of fluid is on the left hand side.

2.1.2 Meshing

One of the most important process of fluid CFD is meshing. The idea of grid emergence is derived from the idea of discretization. Discretization discretizes the continuous solution domain into many finite sub-regions and solves the physical variables of each sub-region separately. Each sub-region is adjacent to continuous and coordinated to achieve the entire variable field (Coordination and continuity). The discrete grid is only a "representation symbol" of physical quantities. The grid is tangible, but the discrete objects can be either tangible (all kinds of solids) or intangible (heat conduction, gas). The most critical core is the mathematical and physical formulae hidden behind the grid. Therefore, to put it simply, the visible grid dispersion is the form, and the invisible physical quantity dispersion is the essential core. For a simple geometry like this research has, block mesh is perfectly competent. The mesh in this simulation is generated so that mesh blocks are evenly distributed before the cylinder for a more precise and even flow rate before the fluid hits the cylinder. Even though vortex shedding is an interesting part of this phenomenon, it doesn't affect the simulation result of the motion of the cylinder. Therefore the mesh after the cylinder is increasing in size gradually. Also, it is expected that there will be no turbulent close to the walls on the side of the geometry, the mesh is also generated in way that the blocks gradually increase in size from the middle towards the walls. Mesh close to the cylinder is the most important part of this simulation, therefore the mesh are generated in a way that the closer to the cylinder's wall, the finer the blocks are.

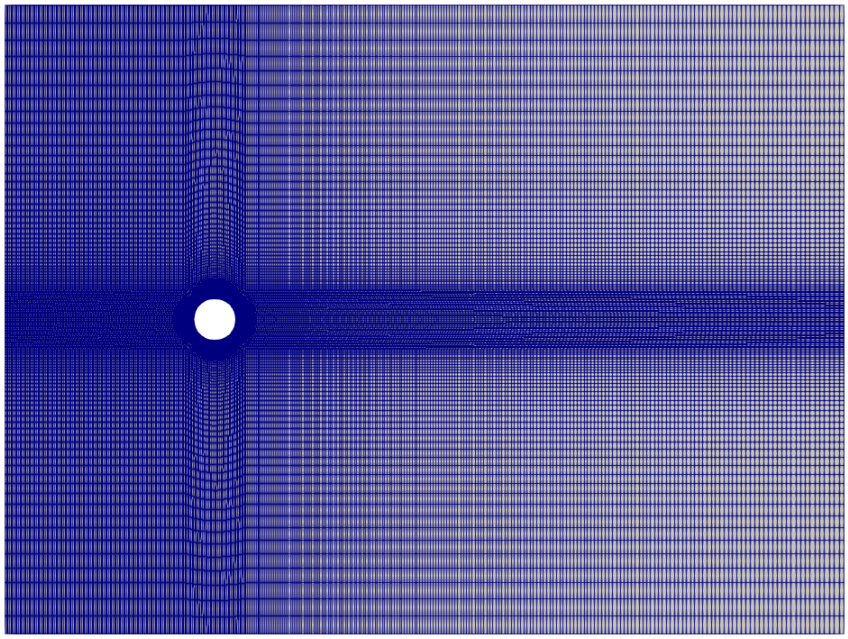

Figure 2.2: A general view of the meshed geometry.

2.1.3 Fluid's Properties

Before the simulation actually takes place, the last thing that needs to be selected for the measurement is the fluid property. For convenience and practicality, the property of water was chosen to be the input values at first, which are $\rho = 997[kg/m^3]$ and $kinematicviscosityk = 1 * 10^{-6}[m^2/s]$. Although for the sake of more straightforward observation and calculation of the behavior, the final kinematic viscosity is $k = 1 * 10^{-5}$, which is ten times more viscous than water. The vortex shedding frequency f is related to the Strouhal number (St) where the Strouhal number depends on the Reynolds number. Therefore the Reynolds should be first determined as[3]:

$$Re = \frac{UD}{k}. \tag{2.1}$$

Since the velocity of the fluid is yet unknown, the Reynolds number is chosen with a practical manner as 100. According to the study made regarding the relationship between Reynolds number and Strouhal number by J. P. Den Hartog[42], even though they are closely related, the Strouhal number varies only between 0.18 and 0.22 in the range of 100 to 100,000 Re. Therefore, the Strouhal number can be first assumed as 0.18 as this is going to be a low Re system, then the vortex shedding frequency is calculated as

$$St = \frac{fD}{U}. \tag{2.2}$$

Assuming $f = 0.1Hz$ for convenience and practical results, velocity is calculated as $U = 0.0222m/s$. It is then rounded to $U = 0.025m/s$ as a more accurate input. Doing with the new defined flow velocity U, Re is calculated again with equation 2.1, resulting $Re = 80$. The vortex shedding frequency can also be approximate with $St = 0.18$,

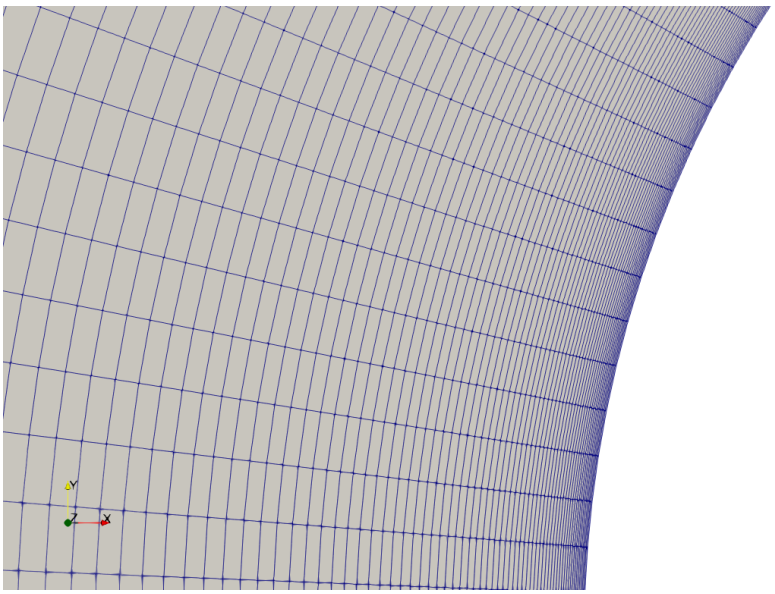

Figure 2.3: Mesh sizing close to the cylinder's wall.

resulting $f = 0.1125Hz$. Here, the velocity ratio should be checked so that it is in a reasonable range. The calculation is done with:

$$U^* = \frac{U}{f_n D}, \tag{2.3}$$

assuming that the cylinder's natural frequency is the same as the calculated vortex shedding frequency, gives the result of $U^* = 5.556$. With the already found relationship between the maximum amplitude and the velocity ratio by Khalak and Williamson[6], the velocity is around $U^* = 5$ so that the upper branch of the relationship will be visible.

A testing simulation is performed, where the cylinder is fixed in the fluid, to check if the vortex shedding occurs as expected. Using the data extracted from the force component, the frequency can be calculated using a Fourier transform. The data collection and calculation here are performed by the built-in software python3 in Ubuntu. The result is as expected, although the actual vortex shedding frequency is at $f = 0.11Hz$ (Figure 2.4). This is a reasonable and acceptable error since the Strouhal number was only chosen numerically. With the actual properties of the vortex shedding, the analytical result of the Strouhal number then is $St = 0.176$. Also, note that the vortex shedding is only visible after around 50 seconds. This is caused by the fluid being static at the beginning of the simulation. The flow rate of the liquid starts building up until it reaches the set amount as equilibrium.

Since the vortex shedding is successfully produced, it is the priority to make the cylinder free in the Y-axis so that oscillation can kick in. To accomplish this, the mesh needs to be adjusted into a dynamic mesh and then constrain its motion on the X and Z axis. The dynamic mesh is created so that within 1 mm from the cylinder wall, the fine mesh will move along with the cylinder itself, giving more accurate calculations. Any mesh outside of the static mesh is compressible and extendable, creating freedom

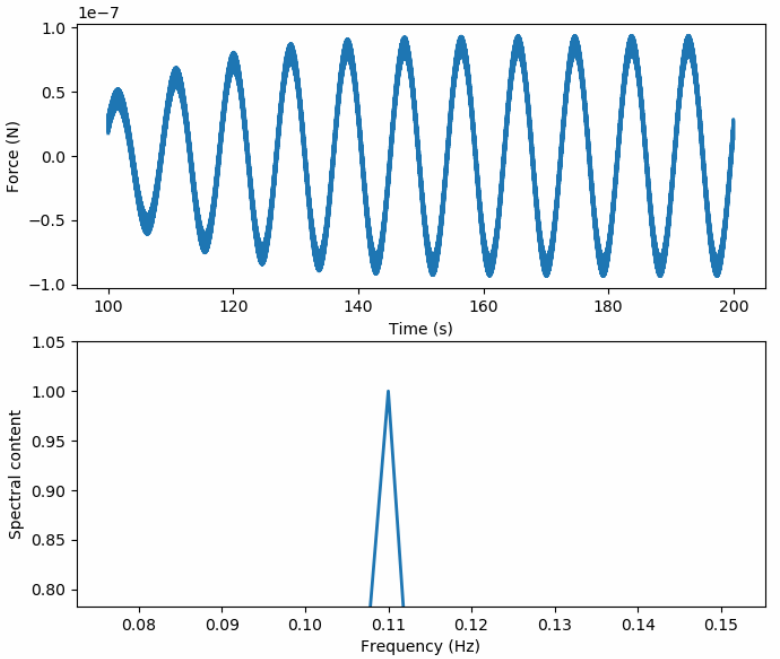

Figure 2.4: The force vs. time plot (top) and the Fourier transform (bottom). The plot of Fourier transform is zoomed in so that the peak is showed clearly.

for the cylinder to have motion[43]. Vibration is created by oscillation between two frequencies, therefore it is necessary to give the cylinder a natural frequency. This can be accomplished by mounting the cylinder elastically with a spring. However, at this point, it is quite interesting to give the system a test run without giving the cylinder any natural frequency.

The result is as expected: although the cylinder is receiving transverse force created by the vortex shedding, it is not tending to move. This result itself is pretty fascinating, but it is now basically a floating object, which does not go into the consideration of the VIV phenomenon.

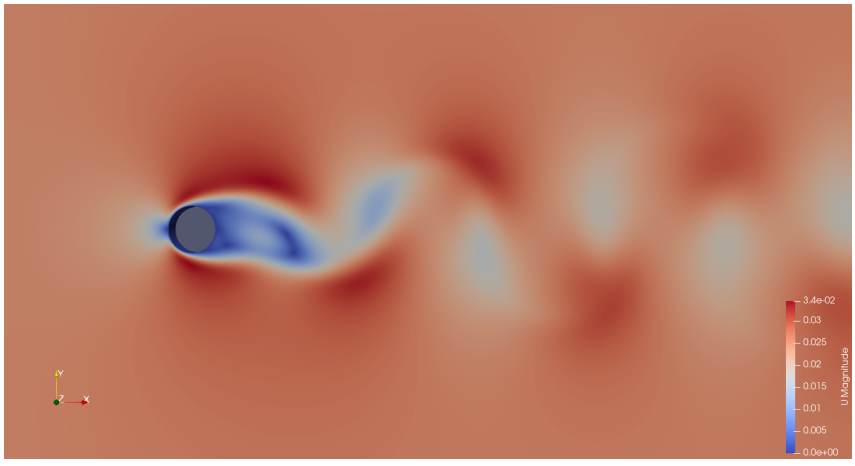

Figure 2.5: With the help of Paraview, the simulation can be seen visibly. The vortex shedding in this simulation results in a 2S wake pattern.

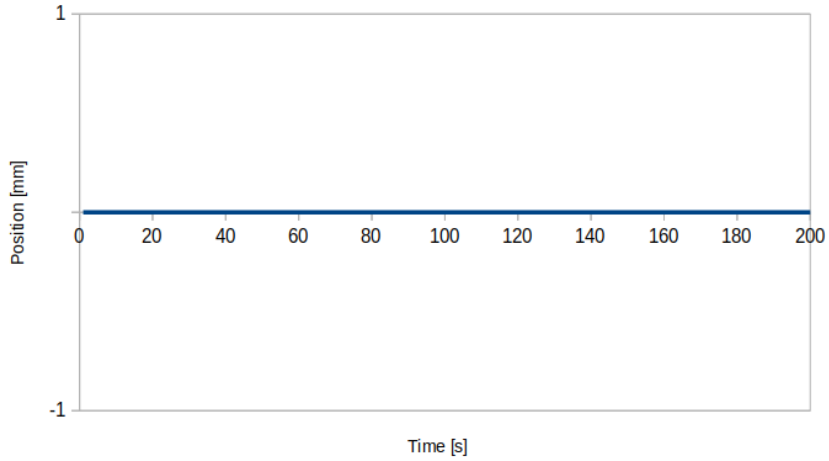

Figure 2.6: The result of when the cylinder is free to move on the transverse direction but does not have a natural frequency, since there is no spring nor restoring force from the cylinder.

2.2 Cylinder's Properties

To achieve the goal of giving the cylinder a same frequency as the shedding frequency, a spring is attached onto the cylinder in the transverse direction. Therefore the natural frequency of a mass∼spring system should be calculated with:

$$\omega = \sqrt{k/m}. \tag{2.4}$$

Where ω is the natural frequency of the body with the unit [radians per second], k is the spring stiffness and m is the mass of the cylinder. Since the result of a Fourier transfer is with the unit [Hz], the ω is converted to f with:

$$f = \frac{\omega}{2\pi}. \tag{2.5}$$

The cylinder's mass is determined so that the mass ratio of the system is about the critical mass ratio of $m^* = 0.54$. The minimum mass of the cylinder then can be calculated as

$$m_{Min} = m^*\pi\rho(D/2)^2L = 0.54 * 997 * 0.02^3 = 0.01353kg \tag{2.6}$$

With the critical mass defined, a set of different mass is create in order to investigate in the behavior of the VIV phenomenon. Which is m =1, 0.75, 0.5, 0.4, 0.3, 0.2, 0.1, 0.09, 0.08, 0.075, 0.07, 0.06, 0.05 [kg].

Although, one crucial matter for any object in a fluid is that the fluid gives it an added mass. It is possible to calculate the added mass m_A with the help of equations mentioned in the introduction, but the process can be easily replaced by a free decay simulation using OpenFOAM. The free decay simulation is essentially giving the spring that's attached to the cylinder a longer rest length at the beginning of the simulation, therefore causing the

cylinder to vibrate and decay in time due to the fluid damping. The added mass has an impact on the natural frequency since there clearly is a mass component in the frequency equation, therefore, using a free decay simulation to approximate the added mass outcome is practical. The basic process of the free decay simulation is:

1. Using the initial mass as a initial guess.
2. Using the wanted natural frequency to calculate the stiffness of the spring k.
3. Running the simulation and plot the result with Fourier transform.
4. With the frequency result in [Hz], calculate the actual mass $(m + m_A)$.
5. Using the new mass as initial guess, then go back to step 2.

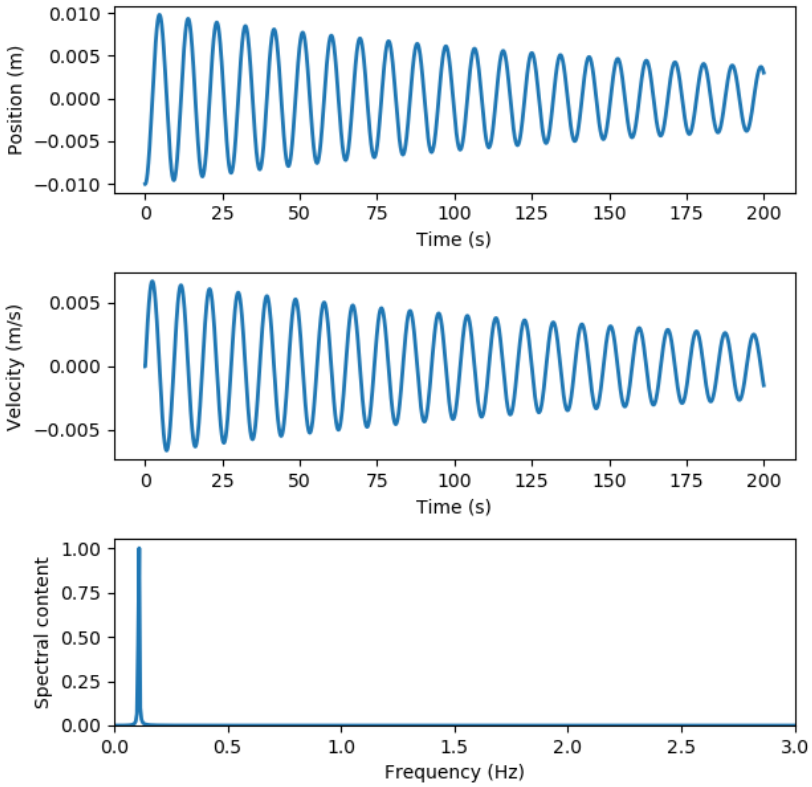

Figure 2.7: An example of the free decay simulation with m=1 kg, plotted with Python.

Performing free decay on every mass gives the result in Table 2.1. The natural frequency of each case are regulated with 0.11 Hz with a maximum error of 1%.

To determine the system's mass damping $((m^* + K_A) * \zeta < 0.05)$, the viscous damping coming from the fluid needs to be also determined. Viscous vibration refers to the movement energy affected by the obstruction caused by the vibration force of the vibrating system that is positive but opposite to the speed. Absorption of secretions exists in the process of internal vibration and shaping. When the fluid vibrates, part of the energy is consumed. In the thermal resistance of an unstable environment, the vibration-generating

m[kg]	$m + m_A$[kg]	k[N/m]
1	1.037	0.4944
0.75	0.7864	0.3757
0.5	0.5346	0.2554
0.4	0.434	0.2073
0.3	0.3313	0.1582
0.2	0.2395	0.1144
0.1	0.134	0.06687
0.09	0.1285	0.0614
0.08	0.1185	0.05662
0.075	0.115	0.05496
0.07	0.109	0.05207
0.06	0.099	0.04279
0.05	0.08913	0.04256

Table 2.1: Free decay results

object is blocked by air or water and converted into energy. With each mass, the viscous damping can be calculated with [44]:

$$n\delta = ln\frac{x_i}{x_{i+n}}, \tag{2.7}$$

$$\zeta = \frac{\delta}{\sqrt{(2\pi)^2 + \delta^2}}. \tag{2.8}$$

Where n is the number of cycle, δ is a logarithmic decrement, x_i is the position at the start of first cycle, and $x_i + n$ is the position at the end of the last cycle. With calculations done, the resulting mass damping of each different mass is shown in Table 2.2.

2.3 Time steps

Time steps give the accuracy of the simulation, and it can be simply explained as the time interval between each calculation. To determine if a time step is good for the simulation, the Courant number can be used. Courant number is a parameter that can give a relative relationship between the time steps and spatial steps. At each calculation, Courant number is calculated by the solver indicating whether the time step is good for the calculation. For a good CFD simulation, the Courant number should definitely stay under 1, and for accurate results, it should be under 0.7 or even lower. During the first simulation, it was found that the Courant number was at a higher number and can sometimes even crash the simulation. For all good reasons, in the control dictionary of the simulation, the maximum allowed Courant number is set to be 0.5. Along with the max-Courant number, adjustable time steps are also turned on. Therefore, the solver will make an automatic decrease in the time step once the Courant number reaches 0.5. In

m[kg]	ζ	$(m^* + K_A) * \zeta$
1	0.00748	0.309
0.75	0.009585	0.3008
0.5	0.01404	0.2996
0.4	0.01726	0.2989
0.3	0.02247	0.2971
0.2	0.0334	0.3193
0.1	0.0567	0.31676
0.09	0.0594	0.3048
0.08	0.6437	0.3045
0.075	0.06896	0.3166
0.07	0.07134	0.3103
0.06	0.07828	0.3093
0.05	0.08615	0.3064

Table 2.2: Mass damping

general, the Courant number is calculated as[45]:

$$C = \Delta t(\sum_{i=1}^{n} \frac{u_{xi}}{\Delta x_i}), \tag{2.9}$$

where Δt is the time step, u is the magnitude of the velocity, x stands for the dimension.

The time step is set to 0.01 seconds in the simulation. However, it is also found that once the mass is too low, it is good to have consistently smaller time steps due to the motion solver algorithm. Therefore the time step for mass lower than 0.3 kg is set to 0.001 seconds, giving more accurate results.

With all the parameters of each case properly checked and set up, the simulation is performed with OpenFOAM's pimpleFoam solver until each has reached the maximum amplitude.

Chapter 3

Data Analysis

3.1 Visualization of the results

Results of the simulation is visualized as plots using Python. For each case with different mass, three important quantities are visualized: position vs. time, velocity vs. time, and the Fourier transformation.

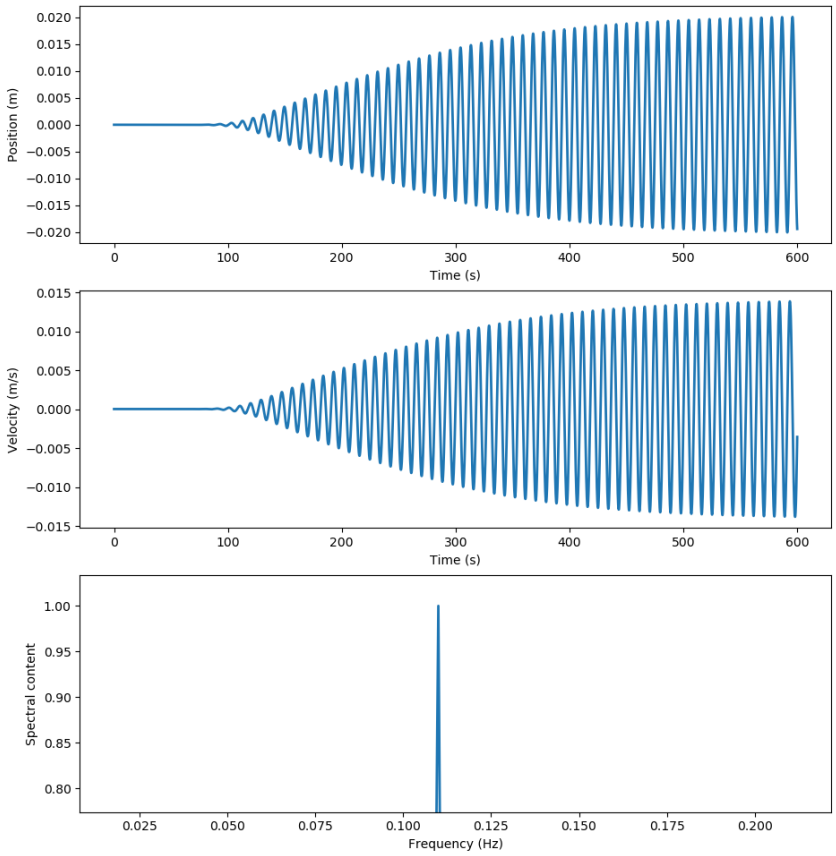

Figure 3.1: Results of case $m = 1$ kg.

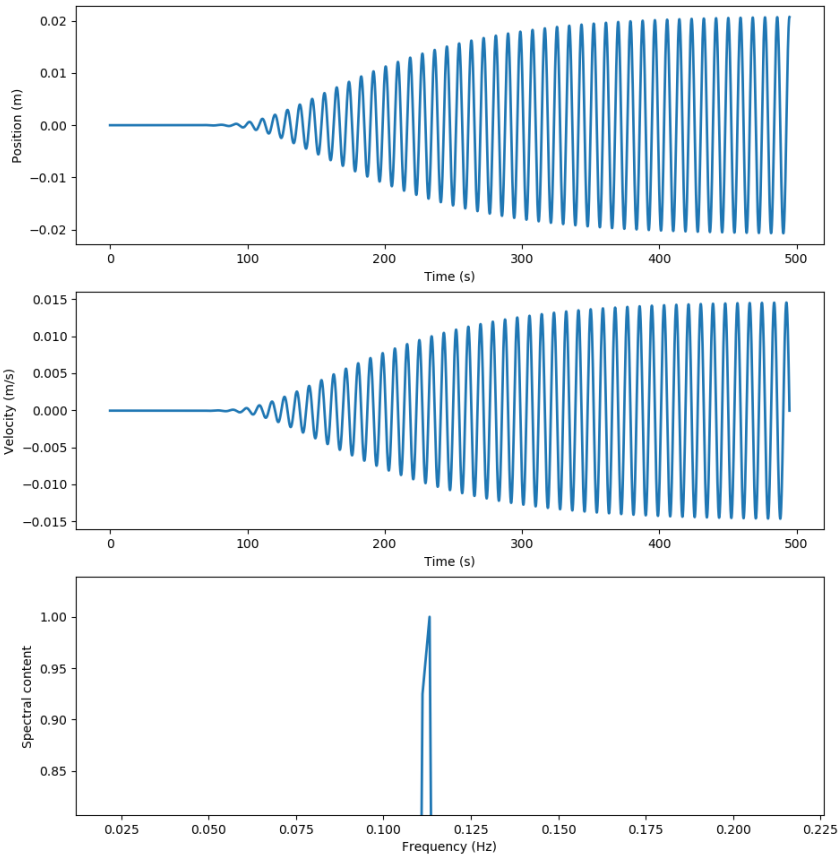

Figure 3.2: Results of case $m = 0.75$ kg.

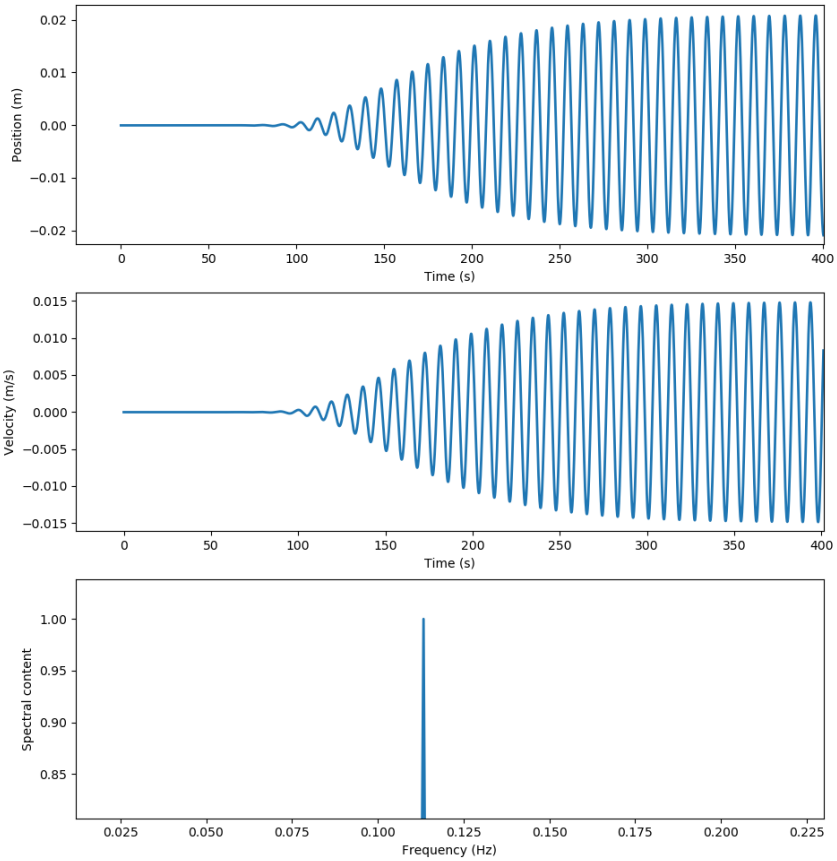

Figure 3.3: Results of case $m = 0.5$ kg.

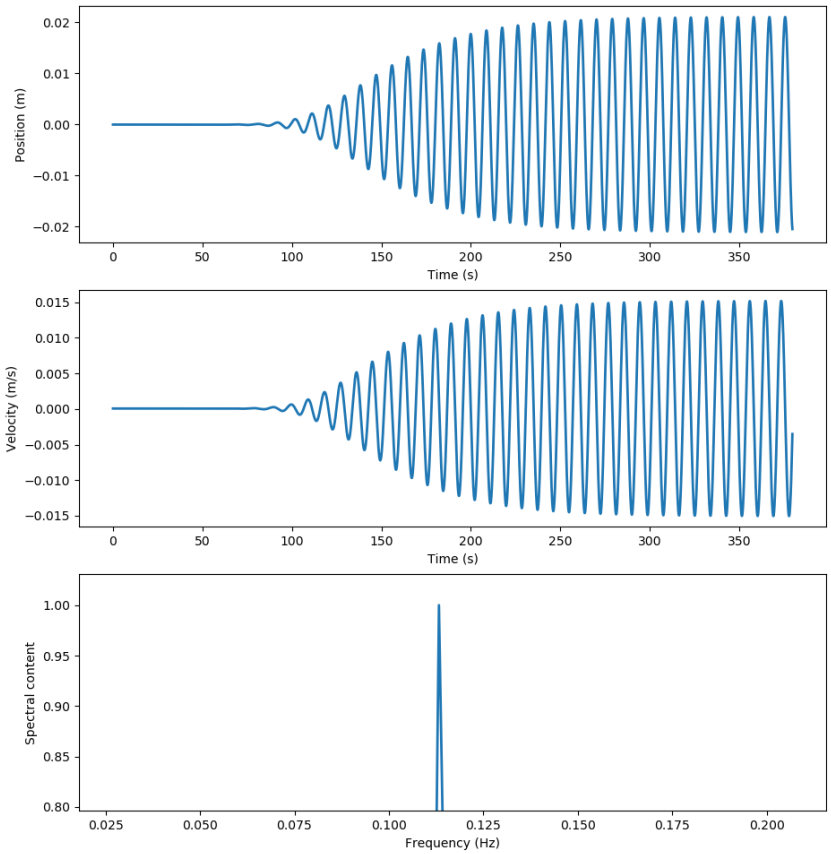

Figure 3.4: Results of case $m = 0.4$ kg.

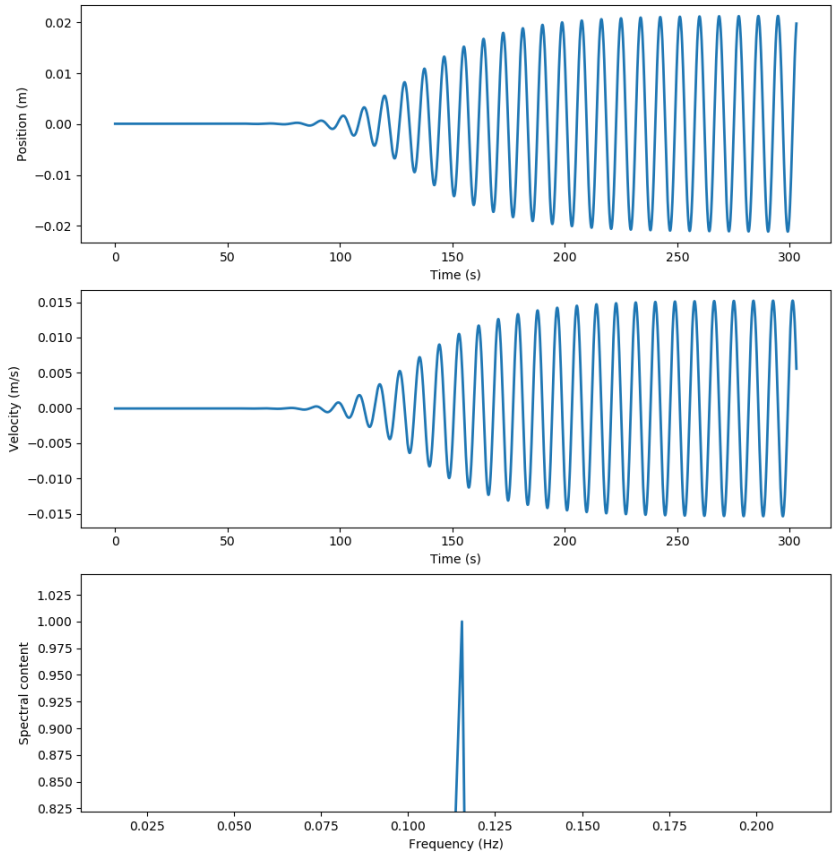

Figure 3.5: Results of case $m = 0.3$ kg.

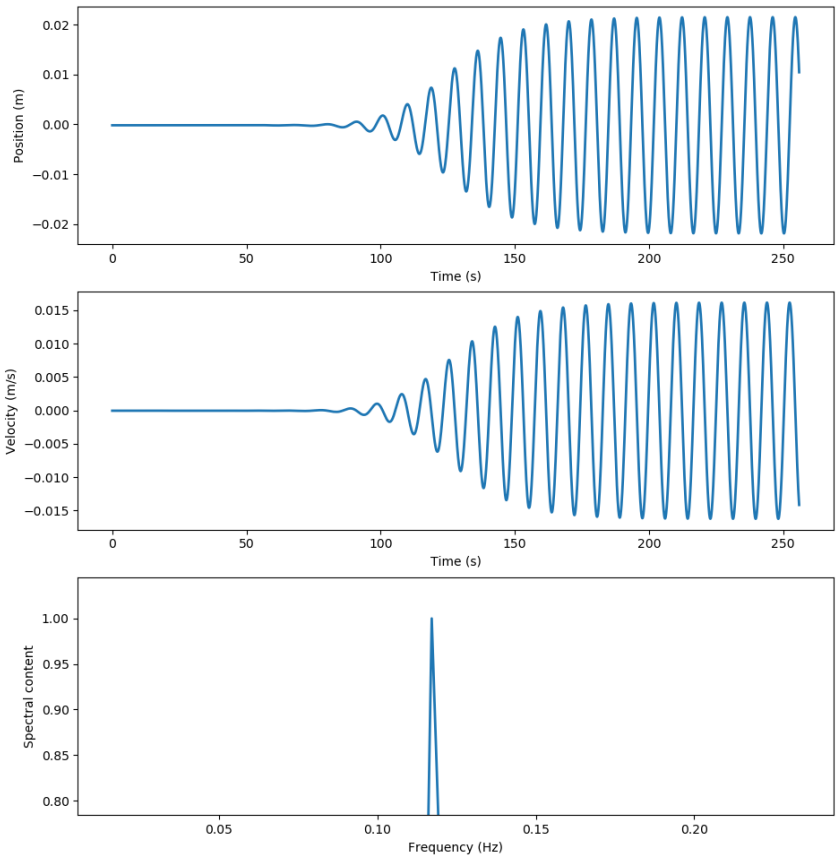

Figure 3.6: Results of case $m = 0.2$ kg.

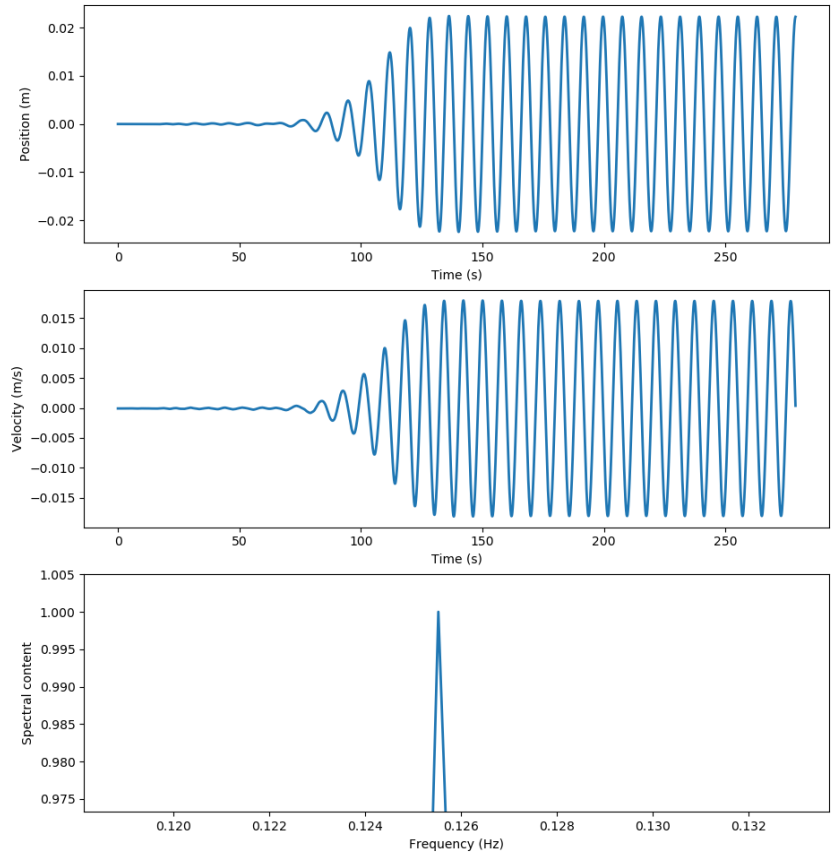

Figure 3.7: Results of case $m = 0.1$ kg.

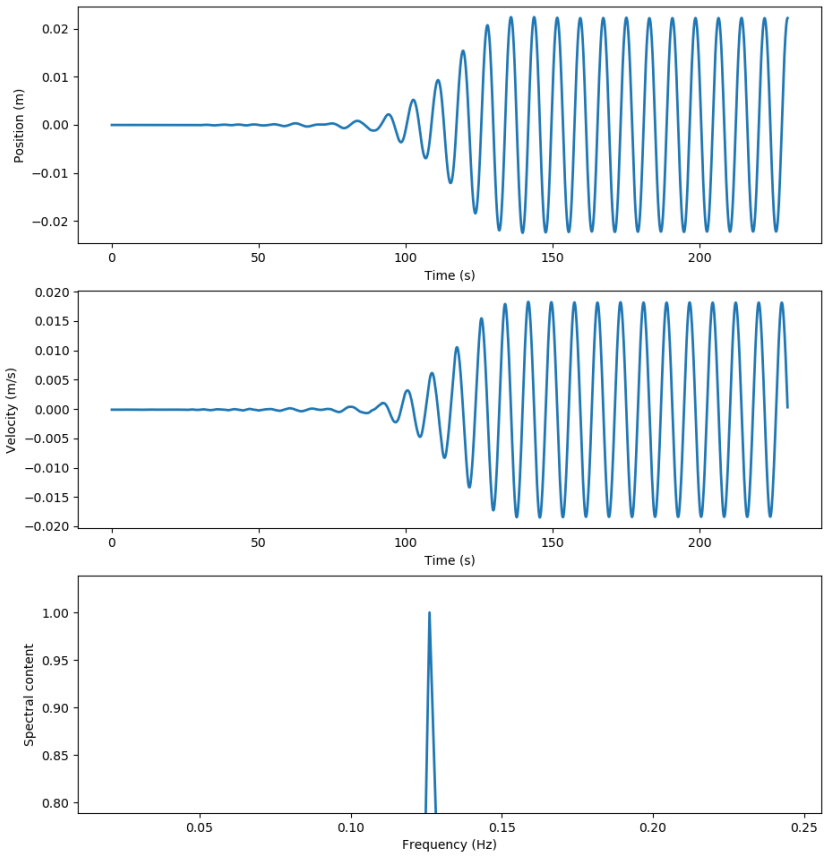

Figure 3.8: Results of case $m = 0.09$ kg.

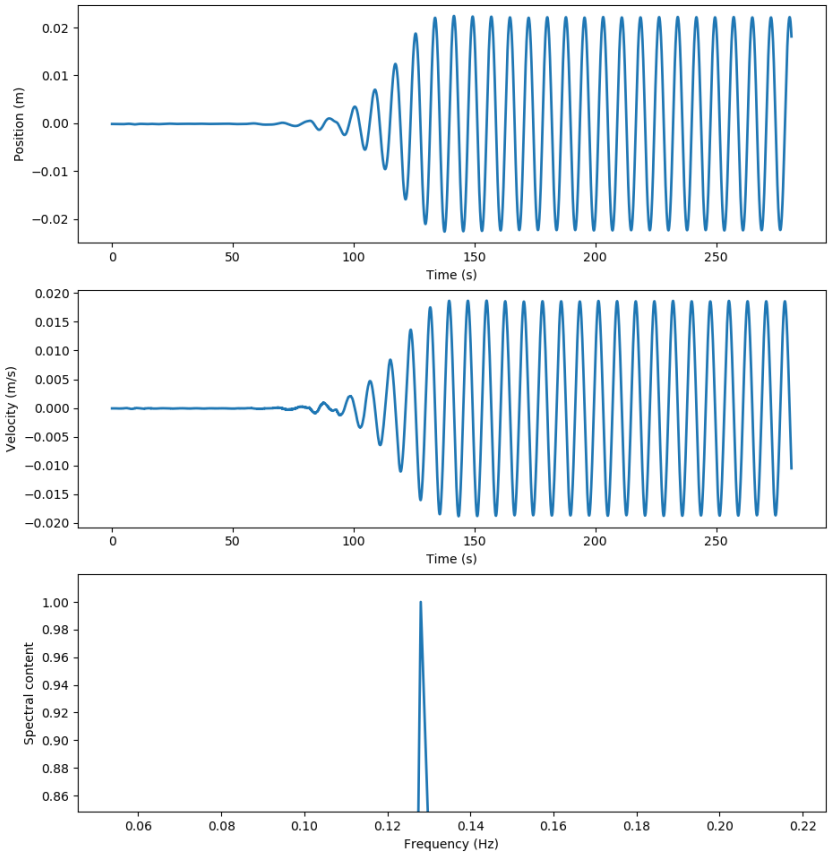

Figure 3.9: Results of case $m = 0.08$ kg.

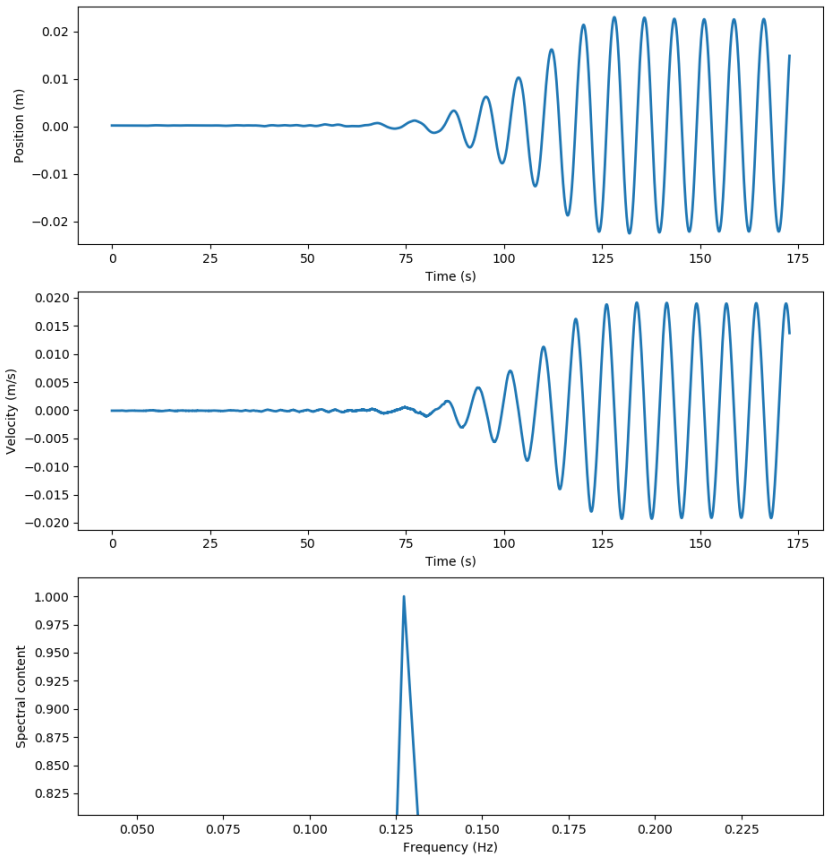

Figure 3.10: Results of case $m = 0.075$ kg.

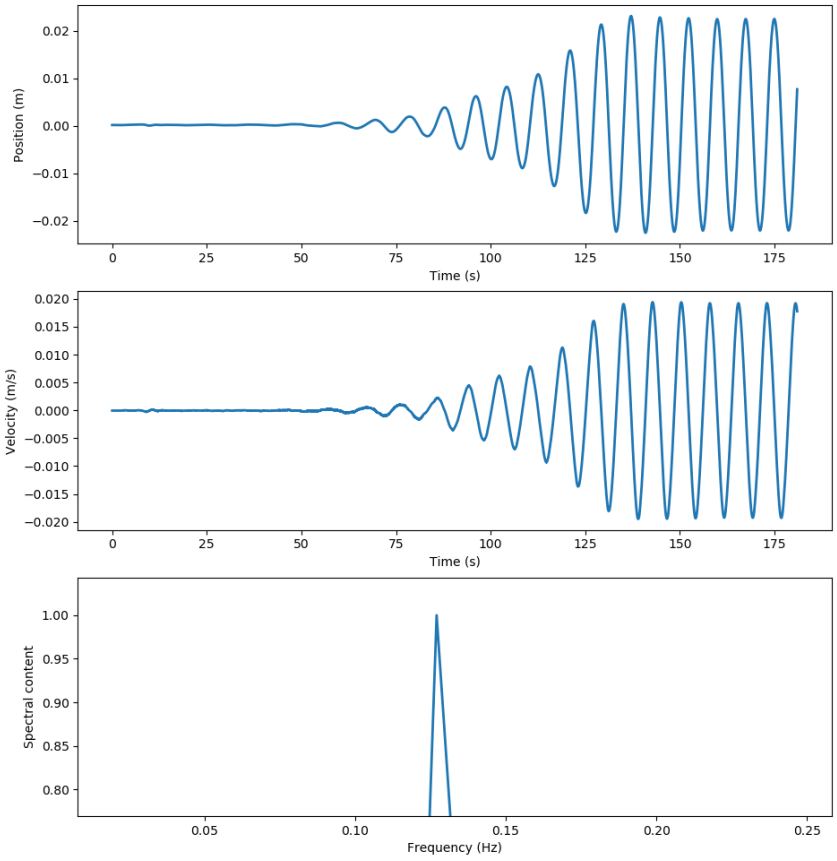

Figure 3.11: Results of case of $m = 0.07$ kg.

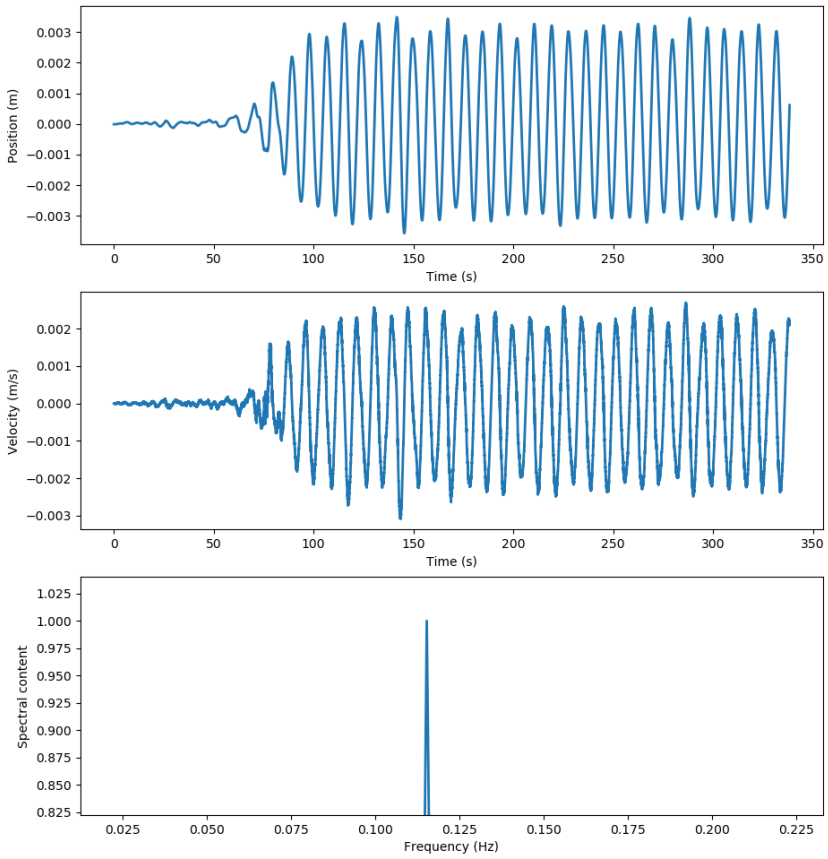

Figure 3.12: Results of case $m = 0.06$ kg.

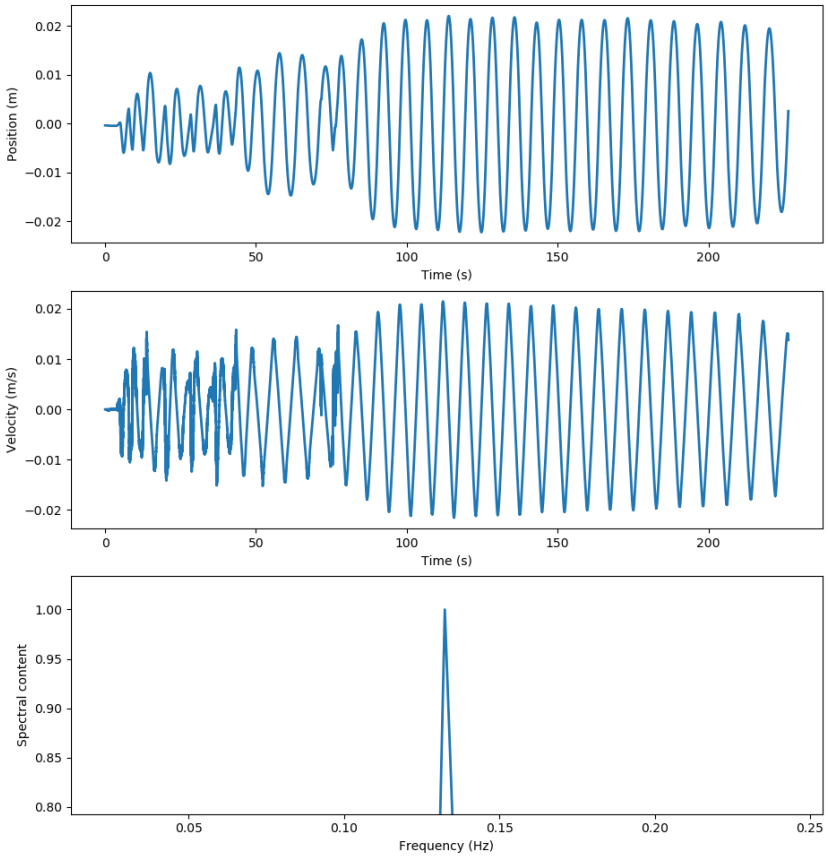

Figure 3.13: Results of case $m = 0.05$ kg.

The length of each case is not the same. This is mainly because the calculation process is considerably long. The result is checked once in a while and stopped when the vibration has reached a reasonably steady amplitude. The spectral content plotted for each case is the result of Fourier transformation, and it is zoomed in for better visual.

3.2 Frequency Ratio

The vibration frequencies obtained from the Fourier transformations for each case can be plotted with respect to the mass ratio with added mass ($m^* + K_A$), which is simply

$$m^* + K_{EA} = \frac{m + m_A}{\pi \rho D^2 L/4}. \tag{3.1}$$

m[kg]	$m^* + K_A$	f	f^*
1	41.3851	0.11	1
0.75	31.384	0.1132	1.029
0.5	21.3351	0.1133	1.03
0.4	17.3201	0.1132	1.029
0.3	13.2217	0.1155	1.05
0.2	9.559	0.1172	1.065
0.1	5.5863	0.1255	1.141
0.09	5.1291	0.1261	1.146
0.08	4.7304	0.128	1.164
0.075	4.5912	0.1273	1.157
0.07	4.35	0.1271	1.155
0.06	3.9509	0.1153	1.048
0.05	3.557	0.1342	1.204

Table 3.1: Mass damping

Although it seems like the vibration is following a trend where the frequency ratio f^* is increasing with a decreasing mass ratio in Figure 3.14, but it is not exactly the case when the mass ratio hits around 4.5. With the cylinder's mass of 0.075 kg and 0.07 kg, it is not clear that the slight decrease of the frequency ratio is caused by uncertainties of the simulation setup. Although when the mass is decreased once more, with $m = 0.06$ kg, a significant decrease of the vibration frequency is found, as in Figure 3.15. Then, at $m = 0.05$ kg, the cylinder vibrates at a significantly higher frequency. Notice that even the mass ratio varies quite a lot between all the cases, the mass damping is almost constant (Table 2.2).

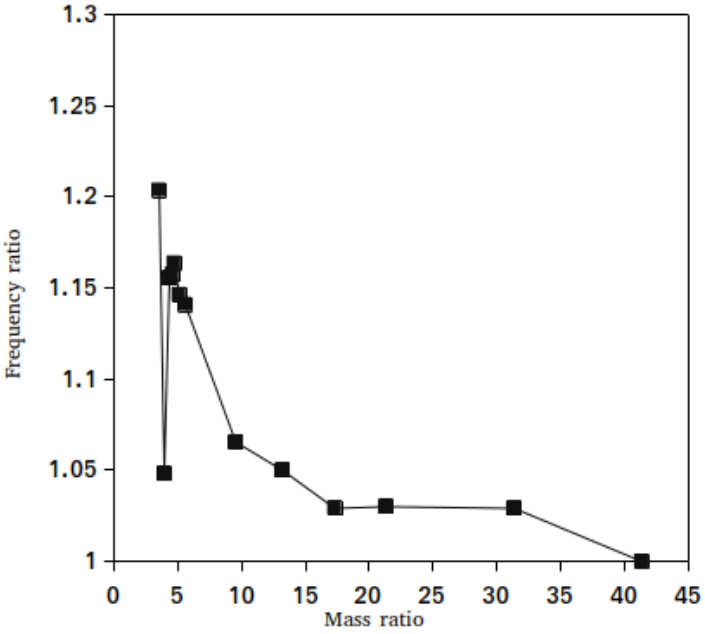

Figure 3.14: Frequency ratio is plotted against the mass ratio.

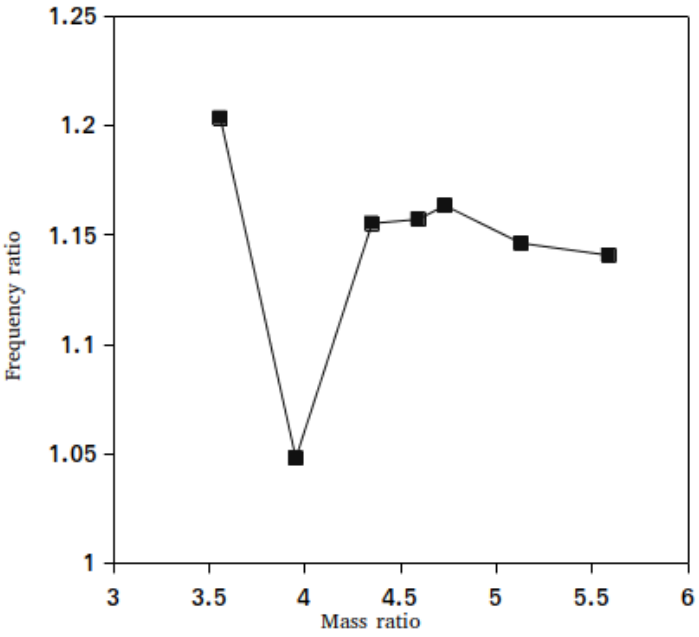

Figure 3.15: A closer look of the plot when mass is under 0.1 kg.

3.3 Settling Time

One of the varying parameters that is changing with different mass ratios is the settling time (t_s) of the vibration. This has never been investigated in previous studies. Once the simulation starts, a constant flow rate is given from the inlet, the vortex shedding phenomenon is only visible after around 50s into the simulation time. The settling time of each case in this research is determined by the first time that a difference of the two peak positions is less than 0.5% of the previous peak Or, in the case of lower mass ratio, the first time that overshoot occurs for the vibration. Overshoot is determined when the peak reaches a higher value than when the vibration settles. The data collected is shown in Table 3.2.

m[kg]	t_s [s]
1	495.588
0.75	405.652
0.5	325.159
0.4	287.823
0.3	242.423
0.2	203.914
0.1	144.155
0.09	143.749
0.08	141.491
0.075	135.771
0.07	137.077

Table 3.2: Settling time

The settling can be plotted against the mass ratio as shown in Figure 3.16. It is found that there is almost a linear relationship between the two parameter. Therefore a trend-line is fitted in and gives the function:

$$t_s(m^*) = 9.893m^* + 99.439. \tag{3.2}$$

Data from 0.06 and 0.05 cases are not included in the plot because of the unstable behavior shown in Figure 3.12 and 3.13. The reason will be analysed in section 3.5

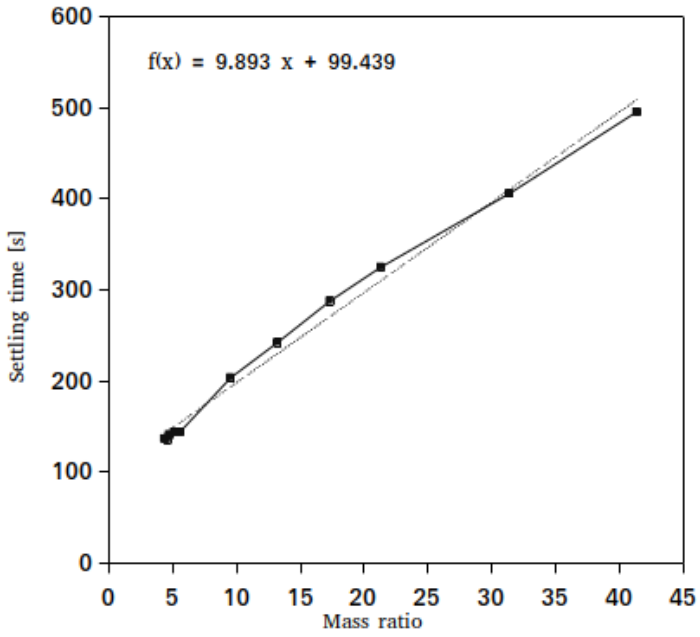

Figure 3.16: Settling time plotted against mass ratio.

3.4 Amplitude Ratio

The maximum amplitude is take where the settling time is. The overshoot amplitude is taken into consideration because it is where damage of the structure can potentially occur. Amplitude ratio is then calculated as

$$Y^* = \frac{y}{D}, \tag{3.3}$$

where y is the maximum amplitude, D is the diameter of the cylinder, which is 0.04 m in this research. This data is collected in Table 3.3 and plotted in Figure 3.17. Note that the data from 0.06 kg and 0.05 kg cases are not plotted for the same reason as the frequency ratio.

m[kg]	y [m]	Y^*
1	0.01939	0.4847
0.75	0.0202	0.505
0.5	0.02053	0.5132
0.4	0.02081	0.5203
0.3	0.02098	0.5245
0.2	0.02159	0.5397
0.1	0.02238	0.5596
0.09	0.02248	0.562
0.08	0.02259	0.5649
0.075	0.02272	0.5679
0.07	0.02295	0.5737

Table 3.3: Amplitude ratio

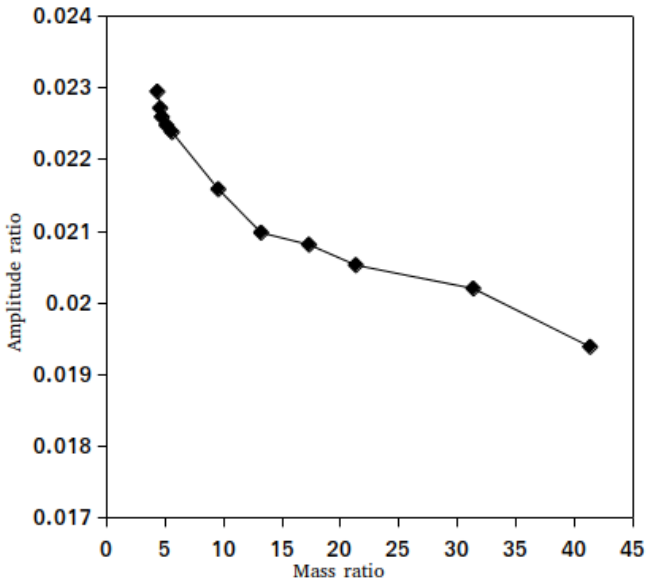

Figure 3.17: Amplitude ratio plotted against mass ratio.

As the mass decreases, the maximum amplitude ratio tends to be increasing rather than Govardhan and Williamson have predicted with the modified Griffin plot. As they have stated that the maximum amplitude at a given Reynolds number and mass damping can be determined regardless of any other parameter with Equation 1.11[33]. Both parameters are constant in this research, but a significant increase of the maximum amplitude can be found with the decreasing mass ratio.

For mass of 0.6 kg and 0.5 kg, the maximum amplitude of the vibration are found to be 0.035 m ($Y^* = 0.0875$) and 0.224m ($Y^* = 0.56$), respectively. It is interesting that it seems like after a certain value, the maximum amplitude has gone down again all the other parameters have increased. Although, it is indeed vibrating at a higher frequency.

3.5 Critical value prediction

With the behavior of settling time, frequency ratio, and amplitude ratio determined and plotted out, a clear change in the behavior can be found around the range of mass of 0.7∼0.5 kg. As for the frequency ratio, significant differences between mass under 0.7 kg. The cylinder vibrates at a higher frequency than any other cases at $m = 0.5$ kg may indicate that the mass ratio is already under its critical value. Looking at its motion from Figure 3.13 also gives the idea that the vibration starts suddenly even when the fluid' flow rate has not yet built up. The vibration also suddenly jumps to a roughly stable amplitude once the velocity is built up to a specific value. This is also another behavior that matches how the cylinder may act under the critical value, as in the response of the cylinder jump from an initial branch to a higher branch as Govardhan and Williamson predicted[8]. For the reasons above, it can be said that the critical mass ratio value of a cylinder that has a mass damping of 0.3 is higher than 3.5 and approximately under 4.35.

Chapter 4

Conclusion

This research has focused on investigating a cylinder with various masses under the phenomenon of VIV with OpenFOAM. Most of the research regarding VIV previously are presented by actual experiments. It is not easy to tell which method is better. For a CFD software, in order to successfully predict the behavior of this phenomenon, there requires several conditions. First of all, as mentioned previously, time step and Courant number are two main parameters that have to be concerned and tested. Secondly, vortex shedding and vortex induced vibration does not occur at any given flow rate of the fluid for a given geometry of the solid. Last but not least, a powerful computer is essential when it comes to extremely small time steps with relatively large motion. However, on the other hand, CFD software such as OpenFOAM provides the ease of controlling those controlled variables such as flow rate and natural frequency with high accuracy. Also, the data is collected efficiently and precisely once the simulation is accurately set up.

The response of the cylinder with a mass of 0.6 kg and 0.5 kg is not accurately shown with the setup of OpenFOAM presently used. Clear, non-periodic, and random vibrations are recorded at the beginning of cases 0.6 kg and 0.5 kg. This is because of the time step is being once again too long against the motion that the cylinder is creating, since the smaller masses are experiencing larger acceleration with the same force. Therefore the Courant number has constantly hitting the maximum of 0.5, which it was set to be. To achieve a more precise simulation result, even lower time steps have to be used. Although, it is going to take a significant longer time for OpenFOAM to perform the calculations or requires the computer to have a much higher performance. For the same reason, the critical value of this research can only be an approximation.

Further study regarding the relationship between maximum amplitude ratio and mass damping parameter can be investigated as there has been found that the amplitude increases even with a constant Reynolds number and mass damping, violating the modified amplitude predicted by Govardhan and Williamson in their research in 2006.

Bibliography

[1] Charles HK Williamson and Anatol Roshko. Vortex formation in the wake of an oscillating cylinder. *Journal of fluids and structures*, 2(4):355–381, 1988.

[2] Owen M Griffin and Steven E Ramberg. The vortex-street wakes of vibrating cylinders. *Journal of Fluid Mechanics*, 66(3):553–576, 1974.

[3] Bruce Roy Munson, Theodore Hisao Okiishi, Wade W Huebsch, and Alric P Rothmayer. *Fluid mechanics*. Wiley Singapore, 2013.

[4] Asif Khalak and Charles HK Williamson. Motions, forces and mode transitions in vortex-induced vibrations at low mass-damping. *Journal of fluids and Structures*, 13(7-8):813–851, 1999.

[5] CC Feng. *The measurement of vortex induced effects in flow past stationary and oscillating circular and D-section cylinders*. PhD thesis, University of British Columbia, 1968.

[6] Asif Khalak and Charles HK Williamson. Investigation of relative effects of mass and damping in vortex-induced vibration of a circular cylinder. *Journal of Wind Engineering and Industrial Aerodynamics*, 69:341–350, 1997.

[7] CHK Williamson and R Govardhan. A brief review of recent results in vortex-induced vibrations. *Journal of Wind engineering and industrial Aerodynamics*, 96(6-7):713–735, 2008.

[8] R Govardhan and CHK Williamson. Modes of vortex formation and frequency response of a freely vibrating cylinder. *Journal of Fluid Mechanics*, 420:85–130, 2000.

[9] FS Hover, AH Techet, and MS Triantafyllou. Forces on oscillating uniform and tapered cylinders in cross flow. *Journal of Fluid Mechanics*, 363:97–114, 1998.

[10] NM Anand and A Torum. Free span vibration of submerged pipelines in steady flow and waves. In *Proc. Intl Symp. Separated Flow Around Mar. Struct*, pages 155–99, 1985.

[11] R Govardhan and CHK Williamson. Resonance forever: existence of a critical mass and an infinite regime of resonance in vortex-induced vibration. *Journal of Fluid Mechanics*, 473:147–166, 2002.

[12] N a Jauvtis and CHK Williamson. The effect of two degrees of freedom on vortex-induced vibration at low mass and damping. *Journal of Fluid Mechanics*, 509:23–62, 2004.

[13] F Flemming and CHK Williamson. Vortex-induced vibrations of a pivoted cylinder. *Journal of Fluid Mechanics*, 522:215–252, 2005.

[14] TL Morse and CHK Williamson. Prediction of vortex-induced vibration response by employing controlled motion. *Journal of Fluid Mechanics*, 634:5–39, 2009.

[15] Sanjay Mittal et al. The critical mass phenomenon in vortex-induced vibration at low. *Journal of Fluid Mechanics*, 820:159–186, 2017.

[16] Richard A Skop and Owen M Griffin. An heuristic model for determining flow-induced vibration of offshore structure. In *Offshore Technology Conference*. OnePetro, 1973.

[17] Richard A Skop. On modeling vortex-excited oscillations. *Naval Research Lab. Report*, 1974.

[18] Owen M Griffin, Richard A Skop, and Steven E Ramberg. The resonant, vortex-excited vibrations of structures and cable systems. In *Offshore Technology Conference*. OnePetro, 1975.

[19] OM Griffin. Vortex-excited cross-flow vibrations of a single cylindrical tube. 1980.

[20] Turgut Sarpkaya. Fluid forces on oscillating cylinders. *Journal of the Waterway, Port, Coastal and Ocean Division*, 104(3):275–290, 1978.

[21] Turgut Sarpkaya. Vortex-induced oscillations: a selective review. 1979.

[22] T Sarpkaya. Offshore hydrodynamics. 1993.

[23] T Sarpkaya. Hydrodynamic damping, flow-induced oscillations, and biharmonic response. 1995.

[24] N Jauvtis and CHK Williamson. Vortex-induced vibration of a cylinder with two degrees of freedom. *Journal of Fluids and Structures*, 17(7):1035–1042, 2003.

[25] N Jauvtis and CHK Williamson. A high-amplitude 2t mode of vortex formation, and the effects of non-harmonic forcing in vortex-induced vibration. *European Journal of Mechanics B/Fluids*, 23:107–114, 2004.

[26] G Moe and T Overvik. Current-induced motions of multiple risers. *BEHAVIOUR OF OFF-SHORE STRUCTURES. VOLUMES 1 and 2., 1983,*, pages 618–642, 1982.

[27] F Angrilli, G Di Silvio, and A Zanardo. Hydroelasticity study of a circular cylinder in a water stream. *Flow-Induced Structural Vibrations*, 1974.

[28] John C Owen, Peter W Bearman, and Albin A Szewczyk. Passive control of viv with drag reduction. *Journal of Fluids and Structures*, 15(3-4):597–605, 2001.

[29] MR Gharib, A Leonard, M Gharib, and A Roshko. The absence of lock-in and the role of mass ratio. In *Proceedings of the 1998 Conference on Bluff-Body Wakes and Vortex-Induced Vibration*. Cornell University Ithaca, 1998.

[30] K Vikestad, JK Vandiver, and CM Larsen. Added mass and oscillation frequency for a circular cylinder subjected to vortex-induced vibrations and external disturbance. *Journal of Fluids and Structures*, 14(7):1071–1088, 2000.

[31] OM Griffin and SE Ramberg. Some recent studies of vortex shedding with application to marine tubulars and risers. 1982.

[32] RA Skop and S Balasubramanian. A new twist on an old model for vortex-excited vibrations. *Journal of Fluids and Structures*, 11(4):395–412, 1997.

[33] RN Govardhan and CHK Williamson. Defining the 'modified griffin plot'in vortex-induced vibration: revealing the effect of reynolds number using controlled damping. *Journal of fluid mechanics*, 561:147–180, 2006.

[34] FS Hover, SN Miller, and MS Triantafyllou. Vortex-induced vibration of marine cables: experiments using force feedback. *Journal of fluids and structures*, 11(3):307–326, 1997.

[35] Petros Anagnostopoulos and PW Bearman. Response characteristics of a vortex-excited cylinder at low reynolds numbers. *Journal of Fluids and Structures*, 6(1):39–50, 1992.

[36] D Jeon and M Gharib. On circular cylinders undergoing two-degree-of-freedom forced motions. *Journal of Fluids and Structures*, 15(3-4):533–541, 2001.

[37] John David Anderson and J Wendt. *Computational fluid dynamics*, volume 206. Springer, 1995.

[38] Hrvoje Jasak, Aleksandar Jemcov, Zeljko Tukovic, et al. Openfoam: A c++ library for complex physics simulations. In *International workshop on coupled methods in numerical dynamics*, volume 1000, pages 1–20. IUC Dubrovnik Croatia, 2007.

[39] Olle Penttinen, Ehsan Yasari, and Håkan Nilsson. A pimplefoam tutorial for channel flow, with respect to different les models. *Practice Periodical on Structural Design and Construction*, 23(2):1–23, 2011.

[40] David C Wilcox et al. *Turbulence modeling for CFD*, volume 2. DCW industries La Canada, CA, 1998.

[41] Pierre Sagaut. *Large eddy simulation for incompressible flows: an introduction*. Springer Science & Business Media, 2006.

[42] Jacob Pieter Den Hartog. *Mechanical vibrations*. Courier Corporation, 1985.

[43] Hrvoje Jasak. Dynamic mesh handling in openfoam. In *47th AIAA aerospace sciences meeting including the new horizons forum and aerospace exposition*, page 341, 2009.

[44] Daniel J Inman and Ramesh Chandra Singh. *Engineering vibration*, volume 3. Prentice Hall Englewood Cliffs, NJ, 2008.

[45] Richard Courant, Kurt Friedrichs, and Hans Lewy. On the partial difference equations of mathematical physics. *IBM journal of Research and Development*, 11(2):215–234, 1967.